Phospholipid flippases and Sfk1 are essential for the retention of ergosterol in the plasma membrane

Takuma Kishimoto[a,*], Tetsuo Mioka[a], Eriko Itoh[a], David E. Williams[b], Raymond J. Andersen[b], and Kazuma Tanaka[a,*]

[a]Division of Molecular Interaction, Institute for Genetic Medicine, Hokkaido University Graduate School of Life Science, Sapporo, Hokkaido 060-0815, Japan; [b]Departments of Chemistry and Earth, Ocean, and Atmospheric Sciences, University of British Columbia, Vancouver, BC V6T 1Z1, Canada

ABSTRACT **Sterols are important lipid components of the plasma membrane (PM) in eukaryotic cells, but it is unknown how the PM retains sterols at a high concentration. Phospholipids are asymmetrically distributed in the PM, and phospholipid flippases play an important role in generating this phospholipid asymmetry. Here, we provide evidence that phospholipid flippases are essential for retaining ergosterol in the PM of yeast. A mutant in three flippases, Dnf1-Lem3, Dnf2-Lem3, and Dnf3-Crf1, and a membrane protein, Sfk1, showed a severe growth defect. We recently identified Sfk1 as a PM protein involved in phospholipid asymmetry. The PM of this mutant showed high permeability and low density. Staining with the sterol probe filipin and the expression of a sterol biosensor revealed that ergosterol was not retained in the PM. Instead, ergosterol accumulated in an esterified form in lipid droplets. We propose that ergosterol is retained in the PM by the asymmetrical distribution of phospholipids and the action of Sfk1. Once phospholipid asymmetry is severely disrupted, sterols might be exposed on the cytoplasmic leaflet of the PM and actively transported to the endoplasmic reticulum by sterol transfer proteins.**

Monitoring Editor
Howard Riezman
University of Geneva

Received: Nov 10, 2020
Revised: May 18, 2021
Accepted: May 21, 2021

This article was published online ahead of print in MBoC in Press (http://www.molbiolcell.org/cgi/doi/10.1091/mbc.E20-11-0699) on May 26, 2021.

Conflict of interest: The authors have no conflict of interest to declare.

*Address correspondence to: Takuma Kishimoto, (kishitaku@igm.hokudai.ac.jp); Kazuma Tanaka (k-tanaka@igm.hokudai.ac.jp).

Abbreviations used: Bio-Ro, biotinylated Ro09-0198 peptide; *CaURA3*, *Candida albicans URA3*; D4, domain 4; DIC, differential interference contrast; DOPC, 1,2-dioleoyl-*sn*-glycero-3-phosphocholine; ER, endoplasmic reticulum; evt-2PH, pleckstrin homology domain of evectin-2; 5-FOA, 5-fluoroorotic acid; GFP, green fluorescent protein; *KlLEU2*, *Kluyveromyces lactis LEU2*; Lact-C2, C2 domain of lactadherin; LD, lipid droplet; Osh, oxysterol-binding protein homologue; P4-ATPases, type 4 P-type ATPases; PapB, papuamide B; pBSK, pBluescript SK+; PBS, phosphate-buffered saline; PC, phosphatidylcholine; PE, phosphatidylethanolamine; PH, pleckstrin homology; PM, plasma membrane; PS, phosphatidylserine; STPs, sterol transfer proteins; TF-Chol, TopFluor-cholesterol; TGN, *trans*-Golgi network; TLC, thin-layer chromatography; ts, temperature sensitive; 3x, triple tandem.

INTRODUCTION

Heterogeneity in the distribution of membrane phospholipids and sterols is essential for the diverse functions of cells. In the plasma membrane (PM) of eukaryotic cells, phosphatidylcholine (PC), sphingolipids, and gangliosides are predominantly distributed in the extracellular leaflet, whereas phosphatidylethanolamine (PE), phosphatidylserine (PS), and other charged lipids are mainly localized to the cytoplasmic leaflet (Zachowski, 1993; van Meer, 2011; Murate *et al*., 2015; Kobayashi and Menon, 2018). This asymmetric distribution of phospholipids is controlled by three types of lipid translocators: flippase, catalyzing inward phospholipid translocation (flip) (Hankins *et al*., 2015; Panatala *et al*., 2015; Andersen *et al*., 2016); floppase, catalyzing outward phospholipid translocation (flop) (Quazi and Molday, 2011; Hankins *et al*., 2015; Neumann *et al*., 2017); and scramblase, catalyzing bidirectional phospholipid translocation (Nagata *et al*., 2020).

Accumulating genetic and biochemical evidence indicates that flippases are integrally linked to phospholipid asymmetry of the organelle membrane from yeast to mammalian cells. Flippases, which

are type 4 P-type ATPases (P4-ATPases), have the ability to translocate phospholipids from the extracellular leaflet of the PM or luminal leaflet of endomembranes to the cytoplasmic leaflet (Panatala *et al.*, 2015). At the cellular level, flippases are associated with diverse physiological functions. Flippases in endomembranes function primarily in membrane trafficking processes (Chen *et al.*, 1999; Gall *et al.*, 2002; Hua *et al.*, 2002; Pomorski *et al.*, 2003; Saito *et al.*, 2004; Furuta *et al.*, 2007; Mioka *et al.*, 2014; Lee *et al.*, 2015; Tanaka *et al.*, 2016), whereas those located in the PM are involved in multiple cellular processes: membrane trafficking (Hua *et al.*, 2002; Pomorski *et al.*, 2003; Furuta *et al.*, 2007; Hachiro *et al.*, 2013), apoptosis signaling (Segawa *et al.*, 2014), mating signaling (Sartorel *et al.*, 2015), the apical membrane barrier (Paulusma *et al.*, 2006), cell polarity (Iwamoto *et al.*, 2004; Saito *et al.*, 2007; Das *et al.*, 2012), and cell migration (Kato *et al.*, 2013).

Flippases form heterodimeric complexes with noncatalytic subunits of the Cdc50 family. Budding yeast has five P4-ATPases: Drs2, Dnf1, Dnf2, Dnf3, and Neo1 (Tanaka *et al.*, 2011) and three Cdc50 family member proteins: Cdc50, Lem3, and Crf1 (Saito *et al.*, 2004; Furuta *et al.*, 2007). Drs2 and Dnf3 interact with Cdc50 and Crf1, respectively, and are mainly localized to the endomembrane, such as the *trans*-Golgi network (TGN) and endosomes. On the other hand, both Dnf1 and Dnf2 form complexes with Lem3 and are mainly localized to the PM (Kato *et al.*, 2002; Pomorski *et al.*, 2003). Except for Neo1, interactions between the P4-ATPases and Cdc50 subunits are essential for endoplasmic reticulum (ER) exit and proper subcellular localization of the complexes but may also contribute to their lipid translocase activity and functions (Saito *et al.*, 2004; Noji *et al.*, 2006; Furuta *et al.*, 2007; Bryde *et al.*, 2010; Takahashi *et al.*, 2011; Puts *et al.*, 2012). Thus, phenotypes in P4-ATPase mutants are phenocopied by their subunit mutants (Saito *et al.*, 2004; Furuta *et al.*, 2007).

Dnf1/2-Lem3 complexes are endocytosed but recycled back to the PM through the endocytic recycling pathway (Saito *et al.*, 2004; Furuta *et al.*, 2007), maintaining the localization of these complexes to the PM. Genetic analyses suggested that the Dnf1/2-Lem3 complexes have PE and PS translocation activity (Kato *et al.*, 2002; Pomorski *et al.*, 2003; Parsons *et al.*, 2006; Stevens *et al.*, 2008). Considering the localization and activity of Dnf1/2-Lem3 complexes, they maintain phospholipid asymmetry predominantly at the PM. Compared to the other four P4-ATPases, little is known about the activity and function of the Dnf3-Crf1 complex. However, the deletion of *DNF3* increases the sensitivity of the *dnf1*Δ *dnf2*Δ double mutant to the PE-binding peptide duramycin (Sartorel *et al.*, 2015), and Dnf3 is implicated in the translocation of PS across the PM (Frøsig *et al.*, 2020), suggesting possible functions of the Dnf3-Crf1 complex in PM phospholipid translocation.

In addition to Dnf1/2-Lem3, some regulators are involved in phospholipid asymmetry of the PM. Serine/threonine kinases Fpk1/2 up-regulate Dnf1/2 flippase activity via phosphorylation (Nakano *et al.*, 2008). Pdr5p and Yor1p, two multidrug ABC transporters (Decottignies *et al.*, 1998; Pomorski *et al.*, 2003), and Opt2, a member of the oligopeptide transporter family (Yamauchi *et al.*, 2015), are implicated in the flop of phospholipids. Recently, we isolated Sfk1 as a multicopy suppressor of the *lem3*Δ mutant; overexpression of Sfk1 suppressed PE and PS exposure in the PM (Mioka *et al.*, 2018). Sfk1 is a conserved transmembrane protein belonging to the TMEM150/FRAG1/DRAM family (Chung *et al.*, 2015). From genetic analyses, we proposed that Sfk1 might negatively regulate the transbilayer movement of phospholipids irrespective of direction in an unprecedented way. The *lem3*Δ *sfk1*Δ double mutant exhibits more severe defects in PE and PS asymmetry in the PM than the *lem3*Δ mutant, and the *lem3*Δ *sfk1*Δ mutant exhibits increased permeability of the PM (Mioka *et al.*, 2018). However, these mutations do not affect cell growth. Given that PM phospholipid asymmetry is commonly observed in eukaryotes, it may be speculated that phospholipid asymmetry plays an important role (e.g., is essential for cell growth). Thus, there might be a gene that functions redundantly with *LEM3* and *SFK1* to control phospholipid asymmetry.

Another important feature of the PM is that this membrane is rich in sterols. Sterols such as mammalian cholesterol and the fungal ergosterol are essential membrane components with tightly controlled homeostasis (Lange and Steck, 2016). At the cellular level, the PM contains approximately 30–40 mol% cholesterol in PM lipids, whereas the ER contains approximately 5 mol% cholesterol (Radhakrishnan *et al.*, 2008; Holthuis and Menon, 2014). Sterols are inserted into lipid membranes through the interaction between 3-hydroxyl groups and hydrocarbon rings of sterols and polar head groups and hydrocarbon chains of phospholipids, respectively (Ali *et al.*, 2007). Each phospholipid has a different affinity for sterols, which determines the strength of their interaction with sterols (Lange and Steck, 2008; Almeida, 2009). Sphingolipids, PC, and PS interact strongly with sterol, whereas phospholipids with small polar head groups and unsaturated fatty acyl tails exhibit weaker interactions (Ramstedt and Slotte, 2006; Lange *et al.*, 2013; Maekawa and Fairn, 2015). Numerous studies have suggested that these interactions contribute to the properties of the PM, including tight packing, high rigidity, and low permeability. However, it is unclear how the PM retains such a high concentration of sterols and whether the asymmetric distribution of PE and PS is involved in retaining sterols in the PM.

In this study, we searched for genes that functionally interact with *LEM3* and *SFK1* by synthetic lethal genetic screening and identified *dnf3* and *crf1* as interacting partners. The conditional *crf1 lem3 sfk1* triple mutant cannot maintain ergosterol in the PM and instead accumulates esterified ergosterol in the lipid droplet (LD). Our results suggest that Dnf1/2-Lem3 and Dnf3-Crf1 flippases and Sfk1 function cooperatively to maintain the phospholipid asymmetry of the PM, which is essential for sterol retention in the PM and thus for the homeostatic control of sterol.

RESULTS

Dnf3-Crf1 flippase is involved in PM phospholipid asymmetry together with Dnf1/2-Lem3 flippases and Sfk1

To isolate genes involved in the regulation of phospholipid asymmetry of the PM in conjunction with Lem3 and Sfk1, we searched for mutations that display synthetic lethality with *lem3*Δ *sfk1*Δ mutations at 30°C. We isolated a new allele of the flippase noncatalytic subunit *crf1* (Figure 1A). To confirm this synthetic lethality, we crossed the *crf1*Δ *lem3*Δ mutant to the *lem3*Δ *sfk1*Δ mutant, followed by tetrad analysis (Supplemental Figure 1, A and B). The *crf1*Δ *lem3*Δ *sfk1*Δ triple mutant did not germinate at 30°C but germinated at 25°C despite severe growth defects (Supplemental Figure 1B), which allowed us to obtain the *crf1*Δ *lem3*Δ *sfk1*Δ triple mutant for further analysis. We next tested the growth of the *crf1*Δ *lem3*Δ *sfk1*Δ triple mutant at 30 and 37°C. The triple mutant grew very slowly at 30°C and showed lethality at 37°C (Figure 1B). The deletion of *DNF3*, which encodes the catalytic subunit of Crf1 (Furuta *et al.*, 2007), also grew poorly when combined with *lem3*Δ *sfk1*Δ (Supplemental Figure 1C).

Dnf3 is mainly localized to endosomal/Golgi membranes (Hua *et al.*, 2002; Pomorski *et al.*, 2003), but it was suggested that Dnf3 also functions at the PM (Frøsig *et al.*, 2020). To examine whether Dnf3-Crf1 is transported to the PM, we used the endocytosis-deficient *vrp1*Δ mutant (Munn *et al.*, 1995). Both Dnf3-3xGFP

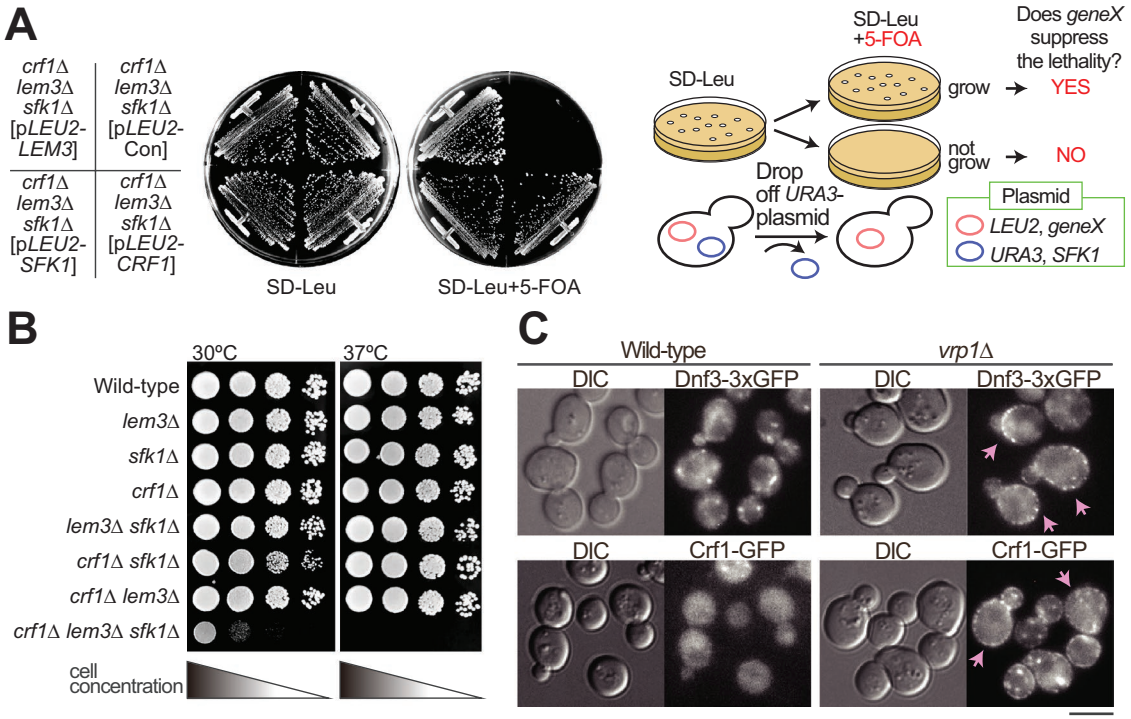

FIGURE 1: Synthetic growth defects of the *crf1*Δ *lem3*Δ *sfk1*Δ mutant. (A) Growth profiles on 5-fluoroorotic acid (5-FOA) plate medium in yeast plasmid shuffling assay. The *crf1*Δ *lem3*Δ *sfk1*Δ mutant harboring pRS316-*SFK1* was transformed with YCplac111 (p*LEU2*-Con), YCplac111-*LEM3* (p*LEU2*-*LEM3*), YCplac111-*CRF1* (p*LEU2*-*CRF1*), or pRS315-*SFK1* (p*LEU2*-*SFK1*). Transformants were streaked onto an SD-Leu + 5-FOA plate and grown at 30°C for 3 d. The cells that require pRS316-*SFK1* for growth are sensitive to 5-FOA because pRS316 contains the *URA3* gene (Boeke *et al.*, 1984). The right panel illustrates this assay system. (B) Growth profiles by spot growth assay. As described in *Materials and Methods*, 10-fold serial dilutions of cell cultures were spotted onto YPDA and grown for 1.5 d at 30 or 37°C. (C) Localizations of Dnf3-3xGFP (triple tandem GFP) and Crf1-GFP in the endocytosis-defective *vrp1*Δ mutant. Cells were grown to mid–log phase in YPDA medium at 30°C. Arrows indicate the cells showing the PM localization of examined proteins. Bar, 5 μm. DIC, differential interference contrast.

(triple tandem green fluorescent protein [GFP]) and Crf1-GFP were localized to intracellular structures but were barely detectable in the PM of the wild type. However, they were observed in the PM when endocytosis was inhibited (Figure 1C). This result indicates that the Dnf3-Crf1 flippase is transported between the PM and endomembranes, similar to Drs2-Cdc50 (Saito *et al.*, 2004). These results raise the possibility that the synthetic growth defect of the *crf1*Δ *lem3*Δ *sfk1*Δ mutant is caused by defects in the PM, and this point was analyzed further.

We attempted to perform phenotypic analysis of the *crf1*Δ *lem3*Δ *sfk1*Δ triple mutant. However, the expression of some GFP-fused proteins resulted in lethality in the *crf1*Δ *lem3*Δ *sfk1*Δ background. Thus, we constructed temperature-sensitive (ts) mutants of *SFK1* by random mutagenesis in the *lem3*Δ *crf1*Δ background as described in *Materials and Methods*. The *crf1*Δ *lem3*Δ *sfk1-2* mutant exhibited acceptable growth at 30°C but a severe growth defect at 37°C (Figure 2A). From the growth profiles of the *crf1*Δ *lem3*Δ *sfk1-2* mutant at 30 and 37°C (Supplemental Figure 2), we analyzed phenotypes of the triple mutant after culturing for 6 h after the shift to 37°C. DNA sequencing of the *sfk1-2* mutant allele revealed that *sfk1-2* contained one mutation that resulted in an amino acid substitution W16R (Figure 2B), which was located in the N-terminal transmembrane region.

Phospholipid asymmetry defects cause the exposure of PS and PE to the extracellular leaflet of the PM. The exposed PS and PE can be indirectly measured by examination of the growth sensitivities of the mutants to the PS-binding cyclodepsipeptide papuamide B (PapB) and PE-binding tetracyclic peptide duramycin. We previously reported that the *lem3*Δ *sfk1*Δ double mutant exhibited high sensitivities to both peptides (Mioka *et al.*, 2018). Thus, we first tested the growth sensitivity of the *crf1*Δ *lem3*Δ *sfk1-2* triple mutant to these peptides at 30°C (Figure 2C). The addition of either the *crf1*Δ or the *dnf3*Δ mutation to the *lem3*Δ mutant elevated the sensitivities to both peptides (Supplemental Figure 3A), consistent with a previous report on the *dnf1*Δ *dnf2*Δ *dnf3*Δ mutant (Sartorel *et al.*, 2015). The *crf1*Δ *lem3*Δ *sfk1-2* mutant did not grow at the concentrations at which the *crf1*Δ *lem3*Δ and *lem3*Δ *sfk1-2* double mutants could grow (Figure 2C). This was confirmed by dose-response growth curve experiment (Supplemental Figure 3B). These results suggest that the *crf1*Δ *lem3*Δ *sfk1-2* triple mutant exposed more PS and PE even at the permissive temperature than did the double mutants. To further confirm the defect in phospholipid asymmetry in the triple mutant, we next visualized the PE exposed to the extracellular surface using the PE-binding biotinylated Ro 09-0198 peptide (Bio-Ro). Fluorescence signals were not detected in either the wild type or the *crf1*Δ *sfk1*Δ double mutant but were detected in both the *crf1*Δ *lem3*Δ (45%) and *lem3*Δ *sfk1*Δ (58%) double mutants (Figure 2D, left and middle panels). In the *crf1*Δ *lem3*Δ *sfk1*Δ triple mutant, the proportion of cells with fluorescence signals increased to 85%. Furthermore, the average signal intensity in the triple mutant was 1.35-fold higher than that in the *lem3*Δ *sfk1*Δ mutant (Figure 2D, right panel).

Next, we examined PS distribution in the cytoplasmic leaflet of the PM in the *crf1*Δ *lem3*Δ *sfk1-2* triple mutant. To visualize PS, we expressed PS biosensors, the C2 domain of lactadherin (Lact-C2)

(Yeung *et al.*, 2008) and the pleckstrin homology (PH) domain of evectin-2 (evt-2PH) (Uchida *et al.*, 2011). GFP-Lact-C2 was mainly distributed in the PM of the examined cells, but intracellular localization was also observed in the triple mutant (Figure 2E, left panel; Supplemental Figure 3C). In contrast, GFP-evt-2PH was normally distributed only to the PM in the wild type and double mutants (more than 96% of cells with PM distribution), whereas the GFP-evt-2PH signal was lost or significantly reduced from the PM in the *crf1*Δ *lem3*Δ *sfk1-2* triple mutant (59% of cells with PM distribution) (Figure 2E, middle and right panels; Supplemental Figure 3D). We speculate that Lact-C2 has a higher affinity for PS, resulting in the detection of a lower level of PS at the PM. Both GFP-Lact-C2 and GFP-evt-2PH were localized to intracellular structures in the triple mutant. However, they appeared to be localized to different structures, which may represent PS-containing membranes or nonspecific protein aggregations. Taken together, these results suggest that the asymmetric distribution of PE and PS was most disturbed in the *crf1*Δ *lem3*Δ *sfk1* triple mutants.

As the Dnf3-Crf1 complex was mainly localized to endosomal/TGN compartments (Figure 1C) (Hua *et al.*, 2002; Pomorski *et al.*, 2003), the *crf1*Δ *lem3*Δ *sfk1-2* mutant may exhibit a defect in membrane trafficking. We examined the localization of the endocytic recycling marker GFP-Snc1, which is mainly localized to polarized PM sites (Lewis *et al.*, 2000), but its localization was not affected in the *crf1*Δ *lem3*Δ *sfk1-2* triple mutant at 37°C (Figure 2F). Similarly, two PM proteins, Pdr5-GFP (ABC transporter) (de Thozee *et al.*, 2007) and Pma1 (H^+-ATPase) (Malinska *et al.*, 2004), were normally transported to the PM in the *crf1*Δ *lem3*Δ *sfk1-2* triple mutant (Figure 2F). We also examined endocytosis in the *crf1*Δ *lem3*Δ *sfk1-2* triple mutant by uptake of the lipophilic dye FM4-64 (Vida and Emr, 1995). The FM4-64 signal was well colocalized to the vacuole membrane marker Vph1-3xGFP (Peters *et al.*, 2001) in both the wild type and *crf1*Δ *lem3*Δ *sfk1-2* triple mutant after 30 min of incubation, suggesting that the triple mutant did not have obvious defects in endocytosis (Figure 2G). These results suggest that the *crf1*Δ *lem3*Δ *sfk1-2* triple mutant is not defective in membrane trafficking to or from the PM.

The PM shows high permeability and low density in the *crf1*Δ *lem3*Δ *sfk1* triple mutants

Phospholipid asymmetry defects may have a profound effect on PM properties. Previously, we showed that the *lem3*Δ *sfk1*Δ double mutant exhibits an increase in membrane permeability by measuring rhodamine dye uptake (Mioka *et al.*, 2018). This experiment was performed in the *crf1*Δ *lem3*Δ *sfk1*Δ triple mutant, and the results suggest that the permeability is further enhanced in the triple mutant compared with that in the *lem3*Δ *sfk1*Δ double mutant (Figure 3A). The large increase in membrane permeability prompted us to examine whether the lipid composition changes in the PM of the *crf1*Δ *lem3*Δ *sfk1-2* triple mutant. We performed sucrose density gradient fractionation to isolate the PM. In the wild type, PM markers, both Pdr5-GFP (de Thozee *et al.*, 2007) and Pma1 (Serrano *et al.*, 1986; Bagnat *et al.*, 2001), were recovered in high-density fractions, whereas Kex2, which is localized to endosomal/TGN compartments (Brickner and Fuller, 1997; Lewis *et al.*, 2000), peaked at a lower density (Figure 3B). However, in the *crf1*Δ *lem3*Δ *sfk1-2* triple mutant, Pdr5-GFP, Pma1, and Kex2 were recovered together in lower-density fractions (fractions 3–9) (Figure 3B). Pdr5-GFP and Pma1 were normally localized to the PM in the *crf1*Δ *lem3*Δ *sfk1-2* triple mutant in microscopic analysis (Figure 2F), suggesting a decrease in PM density, which makes PM isolation from the triple mutant technically challenging. Thus, we measured the phospholipid composition in the total cellular lipids. No significant difference in lipid composition was found in the double and triple mutants (Supplemental Figure 4). These results suggest that a major change occurs in the PM of the *crf1*Δ *lem3*Δ *sfk1* triple mutant.

Isolation of *KES1* as a multicopy suppressor of the *crf1*Δ *lem3*Δ *sfk1-2* mutation

To explore the essential functions of phospholipid asymmetry in the PM, we screened for multicopy suppressors of the ts growth defect of the *crf1*Δ *lem3*Δ *sfk1-2* triple mutant. Multicopy suppressor is a gene whose overexpression suppresses a mutant phenotype. We found that overexpression of *KES1* suppressed the growth defect (Figure 4A). Kes1, also known as Osh4, is an oxysterol-binding protein (OSBP) homologue (Osh) that is implicated in sterol transport within cells (Antonny *et al.*, 2018). Budding yeast contains seven Osh homologues, Osh1–7, that exchange specific lipids between organelles (Lev, 2010). We next tested whether overexpression of other Osh proteins, except for *OSH1*, which localizes to the nucleus–vacuole junction (Manik *et al.*, 2017), could suppress the growth defect of the *crf1*Δ *lem3*Δ *sfk1-2* triple mutant. Only *KES1* overexpression suppressed the ts growth defect of the *crf1*Δ *lem3*Δ *sfk1-2* triple mutant (Figure 4A). Increased rhodamine uptake was also suppressed by *KES1* overexpression in the *crf1*Δ *lem3*Δ *sfk1-2* triple mutant (Figure 4B)

We next examined whether the sterol-binding activity of Kes1 is required to suppress the growth defect of the *crf1*Δ *lem3*Δ *sfk1-2* triple mutant. Overexpression of $KES1^{E117A}$, $KES1^{L111D}$, and $KES1^{Y97F}$, which abolishes the binding of Kes1 to sterols (Im *et al.*, 2005), did not suppress the growth defect of the triple mutant (Figure 4C). Correspondingly, overexpression of $KES1^{L111D}$ did not suppress rhodamine accumulation (Figure 4B, p*Kes1m*). These results suggest that the *crf1*Δ *lem3*Δ *sfk1-2* triple mutant may have a defect in intracellular transport, homeostasis, or distribution of ergosterol.

Ergosterol is reduced in the PM of the *crf1*Δ *lem3*Δ *sfk1* triple mutants

We examined the distribution of ergosterol in the *crf1*Δ *lem3*Δ *sfk1* triple mutants. Filipin is a polyene antibiotic that binds to cholesterol and ergosterol and is used as a probe for cellular sterol distribution (Beh and Rine, 2004; Kishimoto *et al.*, 2016). Wild type and double mutants were evenly labeled with filipin at the PM (Figure 5A: Supplemental Figure 5). However, the *crf1*Δ *lem3*Δ *sfk1*Δ triple mutant drastically decreased filipin labeling to the PM and instead showed the enhancement of intracellular labeling (Figure 5A). Eighty-three percent of the *crf1*Δ *lem3*Δ *sfk1*Δ triple mutant cells clearly displayed the loss or reduction of filipin signal in the PM ($n = 98$ cells). Quantitative analysis of fluorescence images further confirmed the decrease in filipin intensity on the PM in the triple mutant (Figure 5A).

We also examined another sterol biosensor, D4H. A bacterial protein toxin, perfringolysin O, binds to cholesterol via its domain 4 (D4) (Shimada *et al.*, 2002; Johnson *et al.*, 2012). A D4 derivative, D4H ($D4^{D434S}$), has been developed as a more sensitive probe; it binds to liposomes containing 20–30% cholesterol mole concentration (Johnson *et al.*, 2012; Maekawa and Fairn, 2015). Although D4H has recently been used to detect the PM sterol in fission yeast (Marek *et al.*, 2020), D4H has not been applied to budding yeast. We generated two fluorescent protein–conjugated D4Hs, GFP-D4H and GFPenvy-D4H, in which GFPenvy is a photostable dimeric GFP derivative (Slubowski *et al.*, 2015; Bajar *et al.*, 2016). When expressed in wild-type cells, GFP-D4H was localized to the PM in 35% of the cells (Figure 5B). In contrast, GFPenvy-D4H was localized to the PM in 94% of the cells. Interestingly, GFPenvy-D4H showed a characteristic localization pattern; it preferentially localized to

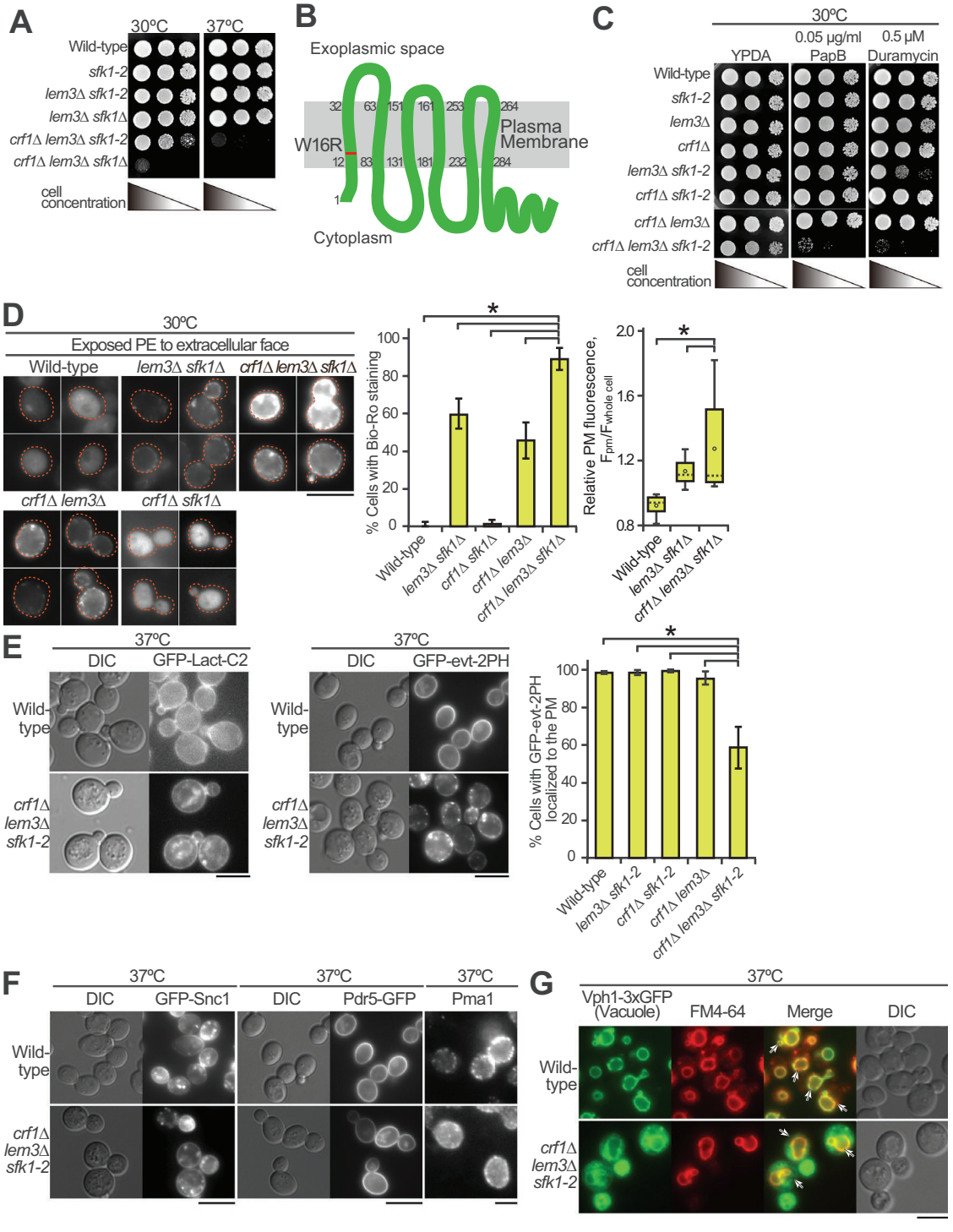

FIGURE 2: The *crf1Δ lem3Δ sfk1* triple mutants show severe defects in phospholipid asymmetry but not in membrane trafficking. (A) Isolation of the *sfk1-2* ts mutant. Tenfold serial dilutions of cell cultures were spotted onto a YPDA plate, followed by incubation at 30 or 37°C for 1.5 d. (B) Amino acid substitution of the Sfk1-2 mutant protein. The W16R substitution occurs in the first transmembrane domain of Sfk1-2. (C) The *crf1Δ lem3Δ sfk1-2* triple mutant was sensitive to PapB and duramycin. Tenfold serial dilutions were spotted onto a YPDA plate containing PapB or duramycin, followed by incubation at 30°C for 2 d. (D) PE was most exposed in the *crf1Δ lem3Δ sfk1Δ* mutant. Left panels: cells were cultured in YPDA at 30°C, and exposed PE was visualized by staining with Bio-Ro and Alexa Fluor 488–labeled streptavidin. Dashed lines indicate cell edges. Middle panel: the percentages of cells showing PE exposure were determined and are expressed as the mean ± SD of three independent experiments ($n > 81$ cells in total for each strain). An asterisk indicates a significant difference, as determined by the Tukey–Kramer test ($p < 0.05$). Right panel: fluorescence intensity at the PM was quantitated as described in *Materials and Methods*. The ratio of the fluorescence at the PM (F_{pm})/that of whole cell ($F_{whole\ cell}$) was determined and is expressed in a boxplot (whiskers: maximum and minimum values; box: first quartile, median, and third quartile; circle: average). The numbers of cells analyzed were 23, 38, and 35 for the wild type, *lem3Δ sfk1Δ*, and *crf1Δ lem3Δ sfk1Δ*, respectively. An asterisk indicates a significant

daughter cells compared with mother cells. This localization pattern is described in the last part of *Results* in more detail.

We next examined the binding activity of recombinant GFP-D4H and GFPenvy-D4H to ergosterol in vitro by liposome sedimentation assay using 1,2-dioleoyl-*sn*-glycero-3-phosphocholine (DOPC) liposomes containing either 50% cholesterol or 50% ergosterol. Consistent with a previous report (Savinov and Heuck, 2017), GFP-D4H bound to ergosterol liposomes at an efficiency of 20% of that to cholesterol liposomes (Figure 5C). On the other hand, GFPenvy-D4H bound to ergosterol liposomes at an efficiency of 56% of that to cholesterol liposomes (Figure 5C), consistent with the results in living cells. The affinity of GFPenvy-D4H to ergosterol was examined with DOPC liposomes containing different concentrations of ergosterol from 10 to 60 mol%. Binding was detected when the ergosterol concentration was 25% or higher (Figure 5D). These results are comparable to the affinity of D4H to cholesterol (Maekawa and Fairn, 2015). The higher affinity of GFPenvy-D4H to ergosterol than GFP-D4H might be because GFPenvy forms a dimeric structure (Bajar *et al.*, 2016).

We next confirmed that GFPenvy-D4H binds to ergosterol in living cells. The *ERG11* gene encodes lanosterol demethylase, which is essential for ergosterol synthesis (Daum *et al.*, 1998). The shutoff of *ERG11* gene expression inhibited the distribution of GFPenvy-D4H to the PM, accompanied by a decrease in free ergosterol levels (Figure 5E; Supplemental Figure 6A). Treatment with the Erg11 inhibitor fluconazole confirmed this observation (Supplemental Figure 6B). We also examined the localization of GFPenvy-D4H in mutants of genes involved in the late steps of the ergosterol biosynthesis pathway (*ERG2-6*) (Munn *et al.*, 1999; Heese-Peck *et al.*, 2002). GFPenvy-D4H was not localized to the PM except for *erg4*Δ, which catalyzes the last step (Supplemental Figure 6C). These results suggest that GFPenvy-D4H is localized to the PM by binding to ergosterol.

We examined the distribution of GFPenvy-D4H in the *crf1*Δ *lem3*Δ *sfk1-2* triple mutant. The localization of GFPenvy-D4H to the PM decreased to some extent in the *lem3*Δ *sfk1-2* and *crf1*Δ *lem3*Δ double mutants, but it drastically decreased to 16% in the *crf1*Δ *lem3*Δ *sfk1-2* triple mutant (Figure 5F; Supplemental Figure 6D). Taking this together with the results of filipin staining, we concluded that ergosterol is significantly lost from the PM in the *crf1*Δ *lem3*Δ *sfk1* triple mutants. Kes1 overexpression increased the PM localization of GFPenvy-D4H from 25 to 55% in the *crf1*Δ *lem3*Δ *sfk1-2* triple mutant (Supplemental Figure 6E). These results suggest that the increased Kes1 enhances ergosterol transport to or inhibits loss of ergosterol from the PM in the triple mutant and that loss of ergosterol from the PM causes phenotypes of the triple mutant, including the growth defect.

We next examined whether exogenously added ergosterol would suppress the growth defect in the *crf1*Δ *lem3*Δ *sfk1-2* triple mutant. We used strains carrying the gain-of-function mutation of a transcription factor *UPC2*, *upc2-1* (G888D), which results in increased uptake of exogenous ergosterol under aerobic conditions

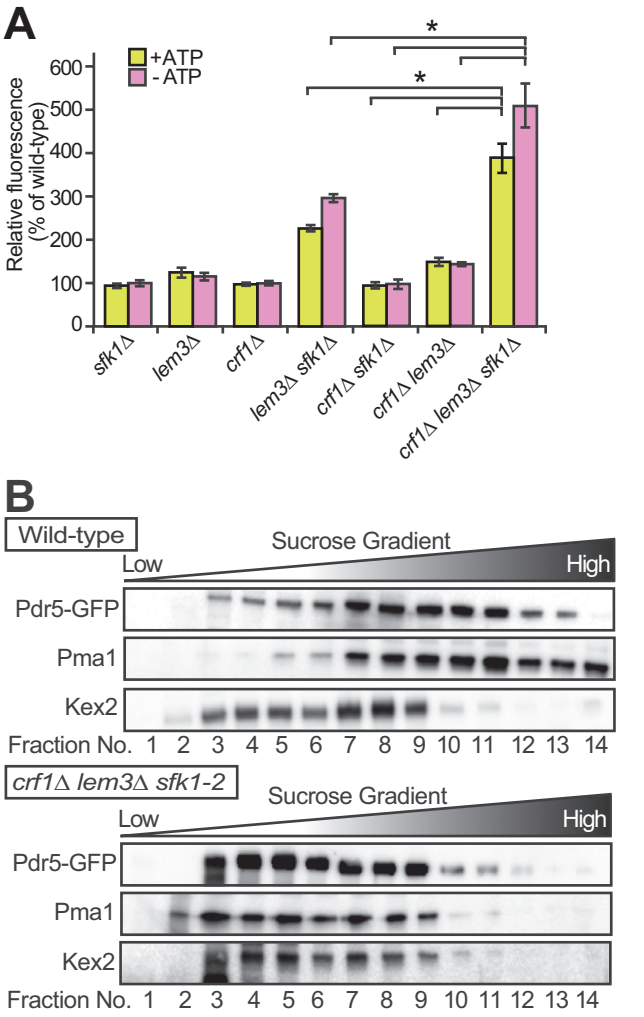

FIGURE 3: Increased permeability and decreased density of the PM in the *crf1*Δ *lem3*Δ *sfk1* triple mutants. (A) Rhodamine uptake is increased in the *crf1*Δ *lem3*Δ *sfk1*Δ triple mutant. Cells were cultured in YPDA medium at 30°C, preincubated in SD medium in the absence (+ATP) or presence (–ATP) of 1 mM sodium azide for 30 min at 30°C, and incubated with rhodamine 6G for 60 min at 30°C. Rhodamine accumulation was measured as described in *Materials and Methods*. Values represent the mean ± SD from three independent experiments. Asterisks indicate a significant difference, as determined by the Tukey–Kramer test ($p < 0.05$). (B) Sucrose density gradient centrifugation analysis of PM proteins, Pdr5-GFP and Pma1, and a TGN/endosome protein, Kex2, in the *crf1*Δ *lem3*Δ *sfk1-2* triple mutant. Cells were cultured as in Figure 2E. Cell lysates were prepared from the wild type and the *crf1*Δ *lem3*Δ *sfk1-2* triple mutant expressing Pdr5-GFP and fractionated in 22–60% sucrose step density gradients as described in *Materials and Methods*. Equivalent volumes from each fraction were subjected to SDS–PAGE, and proteins were detected by immunoblotting.

difference, as determined by the Tukey–Kramer test ($p < 0.05$). (E) GFP-evt-2PH was mislocalized in the *crf1*Δ *lem3*Δ *sfk1-2* mutant. Cells were grown in YPDA medium to mid–log phase at 30°C and then shifted to 37°C, followed by incubation for 6 h. Right panel: the percentage of cells with GFP-evt-2PH at the PM was determined and is expressed as the mean ± SD of three independent experiments ($n > 154$ cells in total for each strain). An asterisk indicates a significant difference, as determined by the Tukey–Kramer test ($p < 0.05$). (F) Normal localization of PM proteins in the *crf1*Δ *lem3*Δ *sfk1-2* mutant. Cells were cultured as in E. Pma1 was detected by immunostaining as described in *Materials and Methods*. (G) Endocytosis was not significantly affected in the *crf1*Δ *lem3*Δ *sfk1-2* mutant. Cells expressing the vacuole membrane marker Vph1-3xGFP were cultured as in E. Then, cells were incubated with FM4-64 on ice for 30 min, followed by incubation at 37°C for 30 min. Arrows indicate the colocalization of FM4-64 and Vph1-3xGFP. Bars, 5 μm.

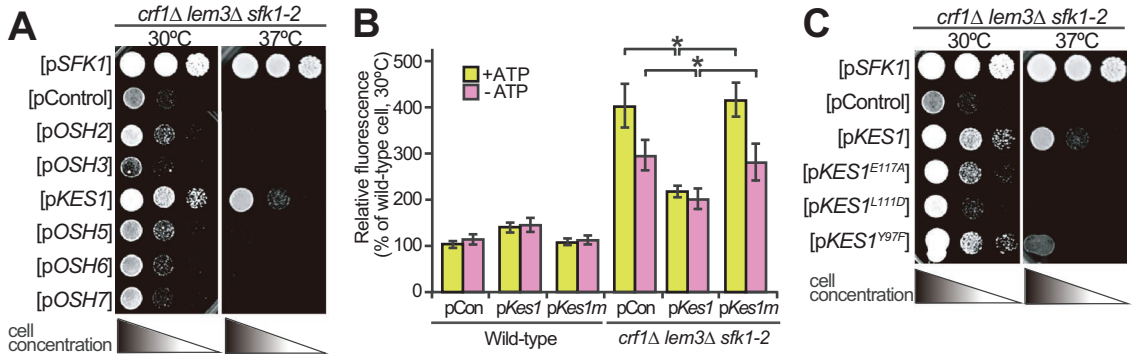

FIGURE 4: Overexpression of *KES1* partially suppresses the phenotypes in the *crf1Δ lem3Δ sfk1-2* triple mutant. (A) Suppression of the growth defect. Cell growth was examined in the *crf1Δ lem3Δ sfk1-2* triple mutant carrying pRS316-*SFK1*, YEplac195, or YEplac195-*OSH2-7*. YEplac195 is a multicopy plasmid. After cells were cultured in SDA-Ura medium at 30°C overnight, 10-fold serial dilutions were spotted onto a YPDA plate, followed by incubation for 2 d at 30 or 37°C. (B) Suppression of high membrane permeability. Rhodamine uptake was examined in the wild type and *crf1Δ lem3Δ sfk1-2* triple mutant harboring YEplac195 (pCon), YEplac195-*KES1* (p*Kes1*), or YEplac195-*KES1*^{L111D} (p*Kes1m*). Cells were cultured as in Figure 2E, except that SDA-Ura medium was used. The rhodamine uptake assay was performed as described in *Materials and Methods*. Rhodamine uptake is represented as a relative value of that (100%) in the wild type harboring YEplac195 incubated at 30°C. Values represent the mean ± SD from three independent experiments. Asterisks indicate a significant difference, as determined by the Tukey–Kramer test ($p < 0.05$). (C) Overexpression of ergosterol binding–deficient *KES1* mutants does not suppress ts growth of the *crf1Δ lem3Δ sfk1-2* triple mutant. Cell growth was examined in the triple mutant transformed with pRS316-*SFK1*, YEplac195, YEplac195-*KES1*, or YEplac195-*KES1* mutants (E117A, L111D, and Y97F). Cells were spotted and grown as in A.

(Lewis *et al.*, 1988; Crowley *et al.*, 1998). The exogenously added ergosterol, which was sufficient to suppress the growth defect of the ergosterol-deficient *hem1Δ* mutant (Georgiev *et al.*, 2011), did not suppress the growth defect of the *crf1Δ lem3Δ sfk1-2* triple mutant even when *KES1* was overexpressed (Figure 6A). We presumed that the triple mutant cannot retain exogenously added ergosterol in the PM. Thus, we monitored the distribution of exogenously added TopFluor-cholesterol (TF-Chol), a fluorescent dye–conjugated cholesterol analogue (Barajas *et al.*, 2014). TF-Chol was retained in the PM of the wild type and double mutants containing *upc2-1* but was not in the *crf1Δ lem3Δ sfk1-2 upc2-1* mutant; only 23% of the triple mutant showed TF-Chol in the PM (Figure 6B; Supplemental Figure 7). TF-Chol appeared to be internalized into the cell to be incorporated into cytoplasmic punctate structures in the *crf1Δ lem3Δ sfk1-2 upc2-1* mutant (Figure 6B). These results suggest that ergosterol is not retained in the PM and that it is transported to intracellular punctate structures in the *crf1Δ lem3Δ sfk1-2* mutant.

Ergosterol is esterified and accumulated in LDs in the *crf1Δ lem3Δ sfk1-2* mutant

The loss of ergosterol in the PM raises a question: where does ergosterol distribute in the cell? We performed thin-layer chromatography (TLC) analysis of total sterols extracted from the cells. In double mutants, the free ergosterol level was approximately 80–85% of that in the wild type, but it decreased to 50% in the *crf1Δ lem3Δ sfk1Δ* triple mutant (Figure 7A). TLC analysis also showed a large increase in esterified ergosterol in the *crf1Δ lem3Δ sfk1Δ* triple mutant. We confirmed that this spot was observed in the wild type at the stationary phase, but not in the acyl-CoA:sterol acyltransferase–deficient *are1Δ are2Δ* mutant (Supplemental Figure 8) (Klug and Daum, 2014). Because esterified ergosterol is the main component of LDs, these results suggest that LDs are increased in the *crf1Δ lem3Δ sfk1Δ* triple mutant. To confirm this, we stained LDs with the lipophilic dye Nile red, which stains neutral lipids in LDs, triacylglycerol and esterified ergosterol (Greenspan *et al.*, 1985). Neither the wild type nor the double mutants showed obvious staining of Nile red, whereas the *crf1Δ lem3Δ sfk1Δ* triple mutant exhibited a clear increase in the number of cells showing Nile red puncta (Figure 7B; Supplemental Figure 9A). We further examined the localization of GFP-tagged LD-related proteins, Tgl1 (steryl ester lipase) (Jandrositz *et al.*, 2005) and Faa4 (long-chain fatty-acid-CoA ligase) (Kurat *et al.*, 2006). The wild type and the double mutants contained a few puncta of these proteins, whereas the numbers of Tgl1-GFP and Faa4-GFP puncta increased 2.5- and 2.8-fold, respectively, in the *crf1Δ lem3Δ sfk1-2* triple mutant compared with those in the wild type (Figure 7C; Supplemental Figure 9B). We confirmed that Tgl1-GFP and Faa4-GFP puncta were colocalized with Nile red–positive puncta; 85% of Tgl1-GFP ($n = 377$) and 88% of Faa4-GFP ($n = 453$) puncta were colocalized with Nile red in the *crf1Δ lem3Δ sfk1-2* triple mutant (Figure 7C). These results suggest that a substantial amount of ergosterol was esterified and accumulated in LDs in the *crf1Δ lem3Δ sfk1* triple mutants.

TF-Chol was also detected in intracellular puncta in the *crf1Δ lem3Δ sfk1-2 upc2-1* mutant (Figure 6B). We next examined whether TF-Chol colocalizes with Faa4-mCherry in the triple mutant. The *crf1Δ lem3Δ sfk1-2 upc2-1* mutant contained approximately 9–14 TF-Chol puncta per cell, and 88% of these puncta ($n = 603$) were colocalized with Faa4-mCherry (Figure 7D).

Taken together, these results suggest that ergosterol is not retained in the PM and is transported to LDs in an esterified form, probably via the ER, in the *crf1Δ lem3Δ sfk1* triple mutants.

The inhibition of sterol esterification partially suppresses growth defects and sterol retention in the PM of the *crf1Δ lem3Δ sfk1-2* mutant

We examined whether inhibition of sterol esterification by mutations in *ARE1*/*ARE2* suppresses the phenotypes of the *crf1Δ lem3Δ sfk1-2* triple mutant. The growth defect of the triple mutant was partially suppressed by the *are2Δ* mutation but not by the *are1Δ*

mutation (Figure 8A). Consistently, Are2 accounts for 65–75% of total cellular acyl-CoA:sterol acyltransferase activity (Yang *et al.*, 1996; Yu *et al.*, 1996). We then examined whether the *are2*Δ mutation restored sterol retention in the PM in the *crf1*Δ *lem3*Δ *sfk1-2* triple mutant. The *are2*Δ mutation increased the number of cells showing the PM localization of GFPenvy-D4H from 17 to 60% in the *crf1*Δ *lem3*Δ *sfk1-2* mutant (Figure 8B). These results are consistent with our notion that loss of ergosterol from the PM is responsible for the growth defect of the *crf1*Δ *lem3*Δ *sfk1-2* triple mutant.

Overexpression of Sfk1 alters the localization of GFPenvy-D4H

The molecular function of Sfk1 remains to be clarified, but our results described above may suggest that Sfk1 is functionally related to ergosterol in the PM. We examined whether a mutation or overexpression of *SFK1* affects the localization of GFPenvy-D4H. Budding yeasts grow by budding, which is a polarized growth of the PM (Figure 9A, right panel). GFPenvy-D4H exhibited polarized localizations in many wild-type cells; it was localized to daughter cells (buds) or near the bud neck in medium- or large-budded cells (Figure 9A, yellow and pink arrows). These results suggest that the accessibility to ergosterol is different between bud and mother PMs because filipin, which was used in fixed cells, evenly stained ergosterol in daughter and mother cells. Interestingly, Sfk1 was mainly localized to mother cells but not to daughter cells, as described previously (Audhya and Emr, 2002), showing a localization pattern opposite to that of GFPenvy-D4H (Figure 9, B and C). The GFPenvy-D4H localizations in large-budded cells were categorized into three patterns: 1) localized throughout the PM (not polarized), 2) localized to the bud and mother cell PM near the bud neck (partially polarized), and 3) localized only to the bud (polarized) (Figure 9A, right panel). These differences may be because GFPenvy-D4H was expressed from a low-copy centromeric plasmid, whose copy number varies among individual cells (Gnügge and Rudolf, 2017). The fluorescence intensity profiles of Sfk1-3xmCherry and GFPenvy-D4H are shown for the "polarized" (Figure 9C) and "partially polarized" (Supplemental Figure 10A) patterns. The proportion of these localization patterns was not changed in the *sfk1*Δ mutant (Figure 9, A and D).

We then examined the effect of *SFK1* overexpression by using a multicopy plasmid carrying *SFK1-mCherry*. Expression from a multicopy plasmid generates heterogeneity in the level of gene expression among individual cells because of variation in plasmid copy number (Caunt *et al.*, 1988). We took advantage of this expression characteristic to examine the correlation between the Sfk1 expression level and the D4H localization pattern. Cells were categorized into high- and low-expression groups based on the fluorescence intensity of Sfk1-mCherry. The relative expression level of *SFK1-mCherry* in highly expressing cells was more than threefold that in lowly expressing cells (Supplemental Figure 10B). In cells lowly expressing Sfk1-mCherry, the GFPenvy-D4H localization pattern was not changed (Figure 9, E, cyan arrows, and F). The mother cell–specific localization pattern of Sfk1-mCherry was not changed in highly expressing cells (Figure 9E, yellow arrows). Interestingly, in cells highly expressing Sfk1-mCherry, GFPenvy-D4H distribution was restricted exclusively to the daughter cells, and those cells that showed the "polarized" pattern were largely increased to 74% (Figure 9F). In these cells, the fluorescence intensity of GFPenvy-D4H was weak in the mother cell PM but increased sharply near the bud neck (Figure 9G). These results suggest that Sfk1 might maintain ergosterol in a state that is inaccessible to GFPenvy-D4H, although its function may be redundant with that of an unknown protein.

DISCUSSION

More than two decades have passed since the first report on the asymmetric distribution of phospholipids in the PM (Zachowski, 1993), but our understanding of its physiological significance is still limited. Our genetic screening reveals that the loss of Dnf1/2-Lem3 and Dnf3-Crf1 flippases and Sfk1 results in severe growth defects, probably due to loss of ergosterol from the PM. The growth defect could be due to increased permeability of the PM or abnormal regulation or/and function of PM proteins. Dnf3 was shown to be involved in some PM functions, including mating pheromone signaling (Sartorel *et al.*, 2015) and pseudohyphal growth (Frøsig *et al.*, 2020), but this is the first demonstration of Dnf3 involvement in essential cell function in a vegetative cell. Because Dnf3 is mainly localized to the TGN, it is also possible that Dnf3 indirectly regulates phospholipid asymmetry in the PM through transport of TGN-derived vesicles. Dnf3 might be also required for transport of an unknown regulator of phospholipid asymmetry to the PM.

Disruption of phospholipid asymmetry is one main reason for the loss of ergosterol from the PM in the triple mutant. Phospholipids interact with sterol via their head groups and acyl chains, which contributes to ordering membrane lipids and securing lipid packing (Mesmin and Maxfield, 2009). In the *crf1*Δ *lem3*Δ *sfk1* triple mutants, PS and PE are more exposed to the extracellular leaflet than in the double mutants and the level of PS in the cytoplasmic leaflet appears to be decreased. Sterols have a higher affinity to phospholipids containing saturated acyl chains than to those containing unsaturated acyl chains (Mesmin and Maxfield, 2009), and PS and PE species in the PM are more abundant in those containing saturated acyl chains than in other organelles in budding yeast (Schneiter *et al.*, 1999). In addition, according to the umbrella model (Mesmin and Maxfield, 2009), phospholipid head groups in the membrane shield nonpolar cholesterol bodies from the aqueous phase. PS with a large head group has a higher affinity for cholesterol than other phospholipids (Maekawa and Fairn, 2015; Nyholm *et al.*, 2019). Therefore, ergosterol, which is also enriched in the cytoplasmic leaflet (Solanko *et al.*, 2018), loses favorable interacting partners in the triple mutant. This would result in a vast increase in "active ergosterol," which may be actively removed from the PM by sterol transfer proteins (STPs) (Figure 10; see below).

Although Sfk1 is implicated in the regulation of phospholipid asymmetry (Figure 2) (Mioka *et al.*, 2018), its protein function remains unknown. Our results that overexpression of Sfk1 excludes GFPenvy-D4H from the mother cell PM suggest that Sfk1 may be functionally relevant to ergosterol. GFPenvy-D4H preferentially localized to the daughter cell PM. However, the ergosterol contents in the cytoplasmic leaflet did not seem to be significantly different between daughter and mother cell PMs because filipin uniformly stained both membranes and because ergosterol is predominantly localized to the cytoplasmic leaflet of the PM, including in mother cells (Solanko *et al.*, 2018). Thus, the differential GFPenvy-D4H localization might reflect different physical states of ergosterol. When sterol levels exceed the interacting capacity of phospholipids in the membrane, a sterol molecule is predicted to be exposed to the surface of the membrane, which increases the chance of its interaction with sterol-sensing proteins. The model defines this behavior as the chemical activation of cholesterol (McConnell and Radhakrishnan, 2003; Maxfield and Menon, 2006; Nelson *et al.*, 2008; Flanagan *et al.*, 2009; Mesmin and Maxfield, 2009; Steck and Lange, 2010). It has been suggested that the D4-containing domain of perfringolysin O preferentially interacts with active cholesterol (Flanagan *et al.*, 2009). Thus, we propose that the chemical activity of ergosterol is

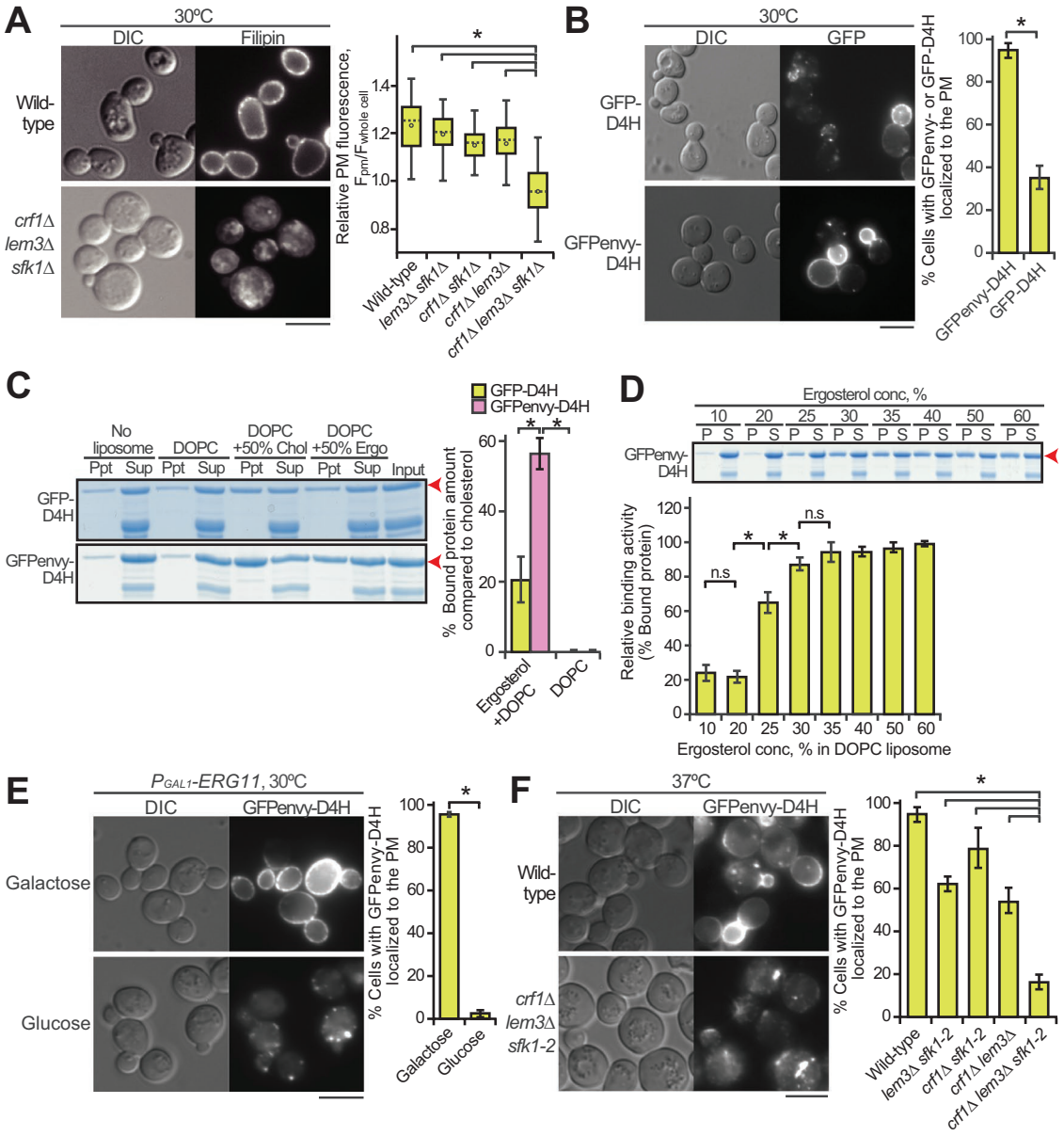

FIGURE 5: Ergosterol is decreased in the PM of the *crf1Δ lem3Δ sfk1* triple mutants. (A) Staining of ergosterol with filipin in the *crf1Δ lem3Δ sfk1Δ* triple mutant. Cells were grown in YPDA at 30°C, and filipin staining was performed as described in *Materials and Methods*. Right panel: fluorescence intensity at the PM was quantitated as described in *Materials and Methods*. The ratio of the fluorescence at the PM (F_{pm})/that of whole cell ($F_{whole\ cell}$) was determined and is expressed with a boxplot (whiskers: maximum and minimum values; box: first quartile, median, and third quartile; circle: average). The numbers of cells analyzed were 100, 100, 99, 97, and 98 for the wild type, *lem3Δ sfk1Δ*, *crf1Δ sfk1Δ*, *crf1Δ lem3Δ*, and *crf1Δ lem3Δ sfk1Δ*, respectively. An asterisk indicates a significant difference, as determined by the Tukey–Kramer test ($p < 0.05$). (B) The distribution of GFP- and GFPenvy-D4H in wild-type cells. Cells harboring pRS316-GFP-D4H or -GFPenvy-D4H were grown in SDA-Ura medium at 30°C to mid–log phase. Right panel: the percentage of cells with GFP- or GFPenvy-D4H at the PM was determined and is expressed as the mean ± SD of three independent experiments ($n > 155$ cells in total for each strain). An asterisk indicates a significant difference, as determined by a two-tailed Student's *t* test ($p < 0.05$). (C) GFPenvy-D4H binds to ergosterol in vitro. The liposome sedimentation assay was performed as described in *Materials and Methods*. Proteins were incubated with liposomes composed of DOPC or DOPC and 50% (mol) ergosterol (Ergo) or cholesterol (Chol) (with corresponding reduction in DOPC), followed by pelleting by centrifugation. Supernatant (Sup) and pellet (Ppt) fractions were separated by SDS–PAGE, followed by staining with Coomassie Brilliant Blue. Arrowheads indicate GFP-D4H or GFPenvy-D4H. A lower band appears to be an incomplete fragment. Right panel: proteins bound to liposomes were quantitated by an image analyzer. The percentage of the bound protein was determined as a relative value of that bound to cholesterol liposomes and is expressed as the mean ± SD of three independent experiments. Asterisks indicate a significant difference, as determined by the Tukey–Kramer test ($p < 0.05$). (D) GFPenvy-D4H binds to DOPC liposomes containing more than 25% ergosterol. A liposome sedimentation assay was performed as in C with DOPC liposomes containing the indicated mol % ergosterol. An arrowhead indicates GFPenvy-D4H. A lower band appears to be an incomplete fragment. The amount of protein

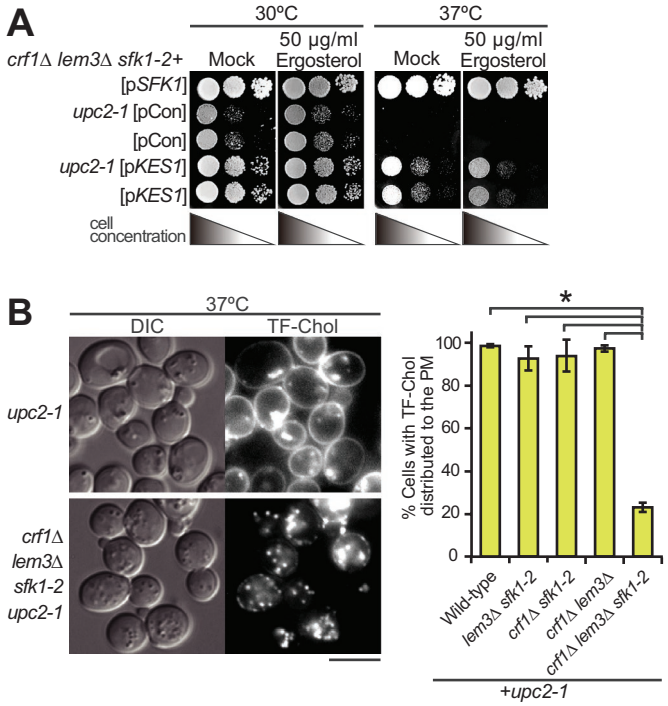

FIGURE 6: Exogenously added ergosterol appears to not be retained in the PM of the *crf1*Δ *lem3*Δ *sfk1-2 upc2-1* mutant. (A) Exogenous ergosterol did not suppress ts growth in the *crf1*Δ *lem3*Δ *sfk1-2 upc2-1* mutant. The *crf1*Δ *lem3*Δ *sfk1-2* mutant with or without the *upc2-1* mutation was transformed with pRS315-*SFK1* (p*SFK1*), YEplac181 (pCon), or YEplac181-*KES1* (p*KES1*). After cells were cultured in SD-Ura-Leu medium at 30°C overnight, 10-fold serial dilutions were spotted onto a YPDA plate containing 0.5% Tween-80 and 0.5% ethanol with or without 50 µg/ml ergosterol, followed by incubation for 1.5 d at 30 or 37°C. (B) TF-Chol is not retained in the PM of the *crf1*Δ *lem3*Δ *sfk1-2 upc2-1* mutant. Left panel: cells were cultured and labeled with TF-Chol as described in *Materials and Methods*. Bar, 5 µm. Right panel: the percentage of cells with TF-Chol at the PM was determined and is expressed as the mean ± SD of three independent experiments ($n > 290$ cells in total for each strain). An asterisk indicates a significant difference, as determined by the Tukey–Kramer test ($p < 0.05$).

higher in the PM of daughter cells than in that of mother cells. The PM of daughter cells is mainly made from newly synthesized lipids by polarized vesicle transport (Pruyne *et al.*, 2004). In this membrane, PE and PS would be exposed to the extracellular leaflet of PM when vesicles are fused with the PM, but they are rapidly flipped to the cytoplasmic leaflet by the action of Dnf1/2-Lem3 flippases, which is localized to the bud PM (Kato *et al.*, 2002; Pomorski *et al.*, 2003). Given the high affinity of PS with ergosterol, PS flipped to the cytoplasmic leaflet may effectively inhibit sterol activation. However, this ongoing process would not ensure that ergosterol molecules are fully kept in an inactive state. In addition, it is possible that ergosterol is also transported to the bud PM by STPs. Therefore, even with such a flippase action, lipids in the bud PM are somewhat agitated during membrane biogenesis, suggesting that sterol activation would not be fully controlled. On the other hand, Sfk1, but not Dnf1/2-Lem3 flippases, is localized to the mother cell PM. Our previous results suggest that Sfk1 represses spontaneous transbilayer movement of phospholipids (Mioka *et al.*, 2018). An interesting possibility is that Sfk1 enhances interactions between ergosterol and phospholipids, which promotes lipid packing in the PM. In such a membrane, lipid movements, including transbilayer movement, would be less active, and sterols would be kept in an inactive state. Because exocytotic vesicle transport and membrane biogenesis do not actively occur in the mother cell PM, phospholipid asymmetry seems to be more established in this membrane. Sfk1 may maintain the established phospholipid asymmetry in a mechanism different from that of flippases and suppress the sterol activation.

The main localization sites were different between Dnf1/2-Lem3 and Sfk1, and the localization of Dnf3-Crf1 in the PM has not been clearly shown in the wild type. However, simultaneous loss of these proteins leads to severe disorganization of the PM, in which active ergosterol would be highly increased due to a reduced shielding effect by phospholipids and reduced lipid packing. The ergosterol in the triple mutant appears to be highly accessible and easily extracted by STPs, resulting in the loss of ergosterol from the PM (Figure 10). Some STPs, including those yet to be identified, seem to be involved in sterol transfer from the PM. These include oxysterol-binding protein homologues (Osh) and lipid transfer proteins anchored at a membrane contact site (LAMs) with StARkin domains (Antonny *et al.*, 2018; Menon, 2018).

Our finding that ergosterol lost from the PM accumulated in LDs as esterified ergosterol is consistent with studies using exogenously added ergosterols (Li and Prinz, 2004; Georgiev *et al.*, 2011). The PM has a much higher ergosterol concentration than the ER, but ergosterol transport by STPs between these membranes is kept in equilibrium because the active ergosterol concentrations seem to be similar in these membranes; the ER membrane contains fewer saturated phospholipids, and thus ergosterol in the ER is not shielded by surrounding phospholipids (Menon, 2018). In the *crf1*Δ *lem3*Δ *sfk1* triple mutants, a vast increase in active ergosterol occurs in the PM, and STPs transport these ergosterols to the ER, in which ergosterol is esterified by Are1/Are2 to form LDs, until the active ergosterol concentration in the PM is balanced with that in the ER.

bound to liposomes is expressed as a relative value (percentage) of that bound to 60% ergosterol liposomes. Values represent the mean ± SD of three independent experiments. "S" and "P" indicate supernatant and pellet fractions, respectively. Asterisks and "n.s." indicate significant and no significant differences as determined by the Tukey–Kramer test (*$p < 0.05$), respectively. (E) The PM localization of GFPenvy-D4H was dependent on ergosterol. *ERG11* was expressed under the control of the glucose-repressible P_{GAL1} promoter. Cells were grown in SGA-Ura medium to mid–log phase at 30°C and then inoculated into fresh galactose (SGA-Ura) or glucose (SDA-Ura) medium, followed by incubation for 12 h at 30°C. Right panel: the percentage of cells with GFPenvy-D4H at the PM was determined and is expressed as the mean ± SD of three independent experiments ($n > 108$ cells in total for each condition). An asterisk indicates a significant difference, as determined by a two-tailed Student's *t* test ($p < 0.05$). (F) GFPenvy-D4H was not localized to the PM in the *crf1*Δ *lem3*Δ *sfk1-2* triple mutant. Cells were cultured as in Figure 2E, except that SDA-Ura medium was used. Right panel: the percentage of cells with GFPenvy-D4H at the PM was determined and is expressed as the mean ± SD of three independent experiments ($n > 253$ cells in total for each strain). An asterisk indicates a significant difference, as determined by the Tukey–Kramer test ($p < 0.05$). Bars, 5 µm.

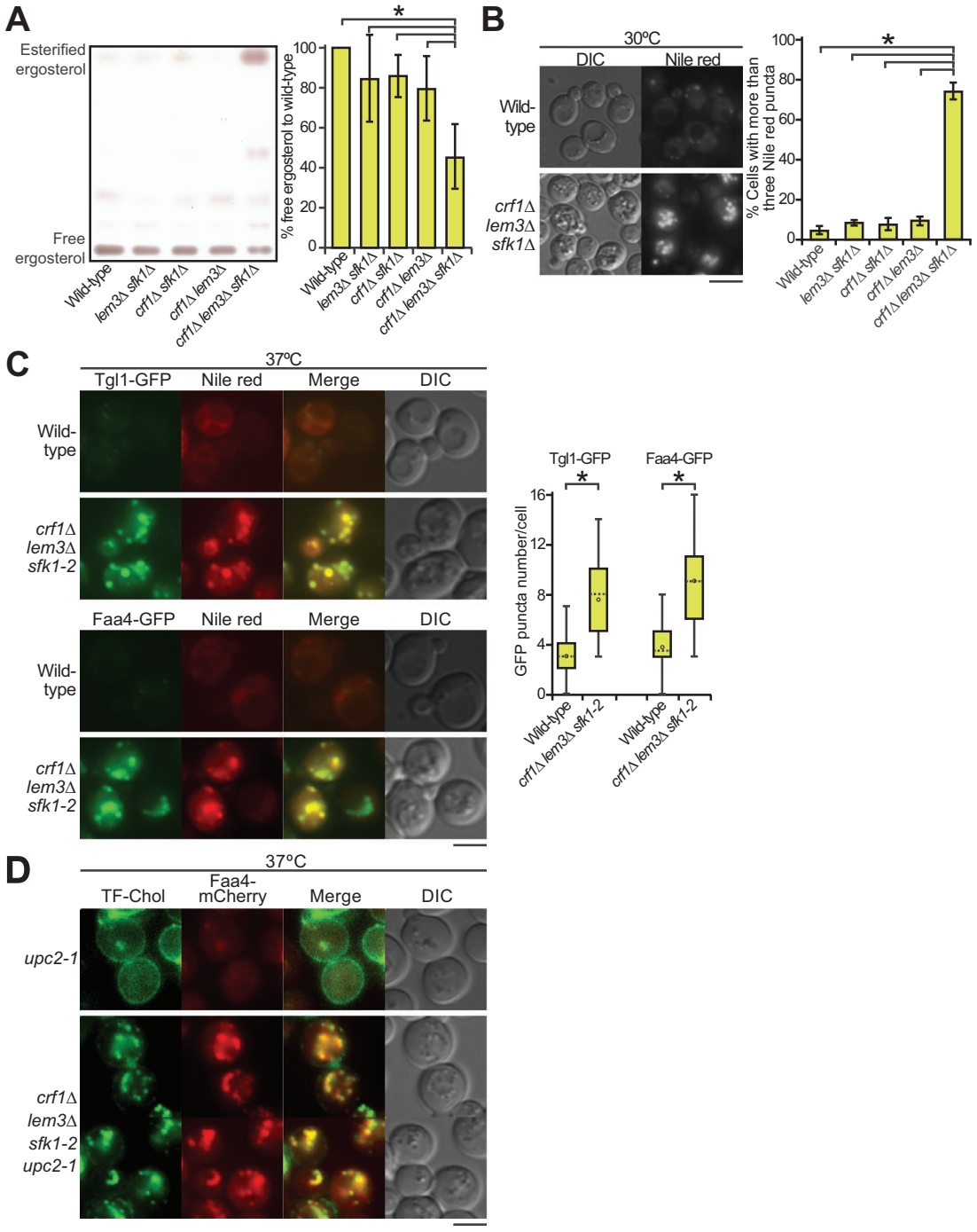

FIGURE 7: LDs were increased in the *crf1Δ lem3Δ sfk1* triple mutants. (A) TLC analysis of total sterols. Ergosterol contents were analyzed by TLC as described in *Materials and Methods*. Right panel: the percentage of free ergosterol relative to that of the wild type was determined and is expressed as the mean ± SD derived from the analysis of six independent samples. An asterisk indicates a significant difference, as determined by the Tukey–Kramer test ($p < 0.05$). (B) Increase in Nile red–positive puncta in the *crf1Δ lem3Δ sfk1Δ* triple mutant. Cells were cultured in YPDA medium to mid–log phase at 30°C, followed by Nile red staining. Nile red staining was performed as described in *Materials and Methods*. Right panel: the percentage of cells with more than three Nile red puncta was determined and is expressed as the mean ± SD of three independent experiments ($n > 315$ cells in total for each strain). An asterisk indicates a significant difference, as determined by the Tukey–Kramer test ($p < 0.05$). (C) Increase in LD marker (Tgl1-GFP and Faa4-GFP)-containing structures in the *crf1Δ lem3Δ sfk1-2* triple mutant. Cells were cultured as in Figure 2E, followed by Nile red staining. Right panel: the Tgl1-GFP or Faa4-GFP puncta were counted in a single focal plane of each cell and are expressed with boxplots (whiskers: maximum and minimum values; box: first quartile, median, and third quartile; circle: average). The numbers of cells analyzed were 51 and 50 (wild type) and 53 and 51 (triple mutant) for Tgl1-GFP and Faa4-GFP, respectively. Asterisks indicate a significant difference, as determined by a two-tailed Student's *t* test ($p < 0.05$). (D) Colocalization of TF-Chol puncta with Faa4-mCherry in the *crf1Δ lem3Δ sfk1-2 upc2-1* mutant. Cells were cultured as in Figure 2E, except that YPDA medium containing TF-Chol was used. Bars, 5 μm.

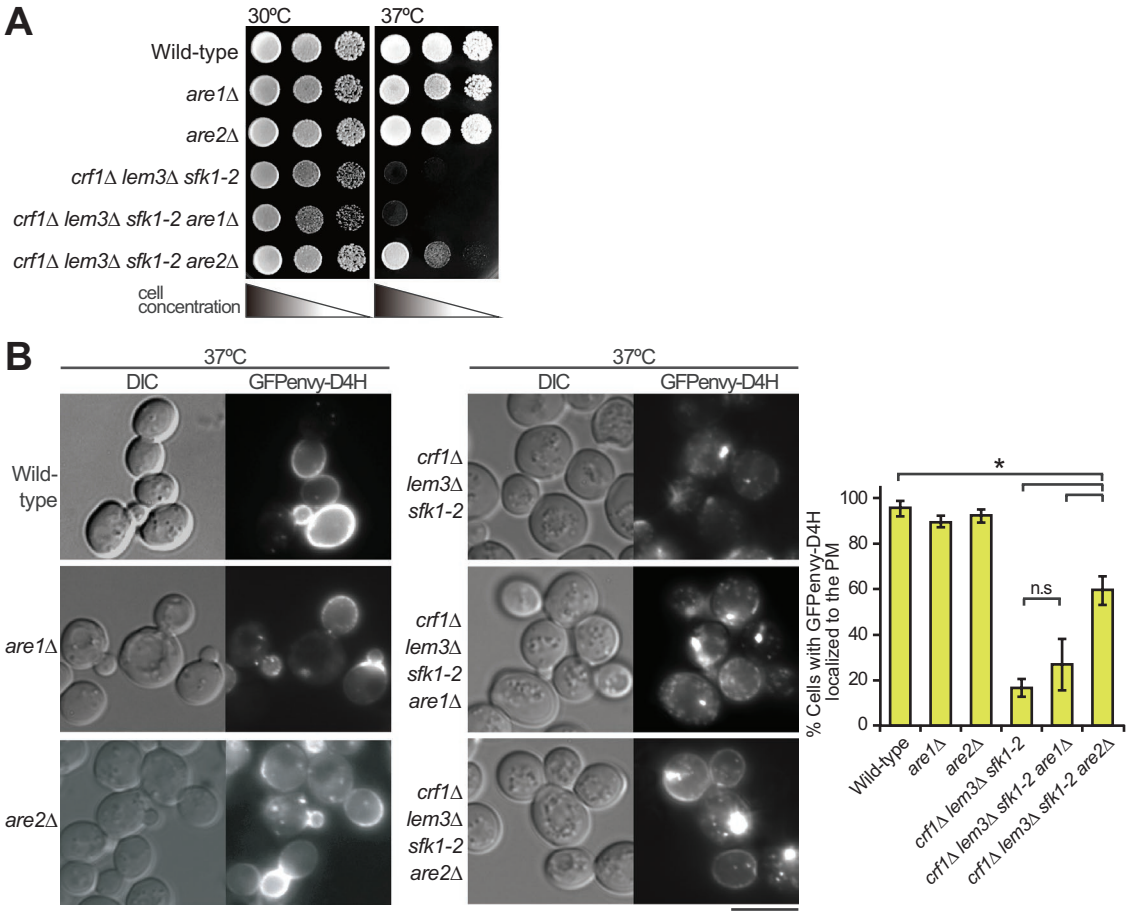

FIGURE 8: The *are2*Δ mutation partially restores ergosterol in the PM of the *crf1*Δ *lem3*Δ *sfk1-2* triple mutant. (A) Suppression of the growth defect. Tenfold serial dilutions were spotted onto a YPDA plate, followed by incubation for 1.5 d at 30 or 37°C. (B) Restoration of GFPenvy-D4H localization to the PM. Cells were cultured as in Figure 2E except that SDA-Ura medium was used. Bar, 5 μm. Right panel: the percentage of cells with GFPenvy-D4H at the PM was determined and is expressed as the mean ± SD of three independent experiments ($n > 219$ cells in total for each strain). Asterisks and "n.s." indicate significant and not significant differences as determined by the Tukey–Kramer test (*$p < 0.05$), respectively.

The *are2*Δ mutation increases active ergosterol in the ER due to defective esterification, and this ergosterol would be transferred to the PM, resulting in the partial suppression of growth defects in the triple mutant.

How sterols are maintained at a high concentration in the PM has been a long-standing question in membrane biology. Phospholipid asymmetry, a conserved feature in the PM, has been implicated in this role (Panatala *et al.*, 2015), but genetic analyses of flippases did not clearly demonstrate that they function in the retention of sterols in the PM. Our results have revealed that flippases actually play an essential role in retaining ergosterol in the PM, but the identification of an additional factor, Sfk1, which is totally different from flippases, was essential. It seems that yeast cells have acquired a robust system to retain an important molecule, ergosterol, in the PM. Our work indicates that unbiased genetic screening is a powerful approach to understanding cellular mechanisms that are regulated by a different set of proteins. Because Sfk1 is conserved as TMEM150A in mammalian cells (Chung *et al.*, 2015), cholesterol might be retained in the PM via a similar mechanism.

MATERIALS AND METHODS

Request a protocol through *Bio-protocol*.

Media and chemicals

General chemicals were purchased from Wako Pure Chemicals Industry (Osaka, Japan) unless otherwise stated. Papuamide B was from the collection of R. Andersen (University of British Columbia, Canada). Duramycin was purchased from Sigma-Aldrich (St. Louis, MO). Yeast strains were grown in YPDA-rich medium (1% yeast extract [Difco Laboratories, Detroit, MI], 2% Bactopeptone [Difco], 2% glucose, and 0.01% adenine). Strains carrying plasmids were grown in SD synthetic medium (0.67% yeast nitrogen base without amino acids [Difco] and 2% glucose) that contained the required nutritional supplements (Rose, 1990). The SDA medium was SD medium that contained 0.5% casamino acid (Difco). For the induction of the *GAL1* promoter, 3% galactose and 0.2% sucrose were used as carbon sources (YPGA and SGA-Ura media).

Yeast strain manipulations and plasmid construction

The yeast strains and plasmids used in this study are listed in Supplemental Tables 1 and 2, respectively. Standard genetic manipulations of yeast strains were performed according to previously described methods (Guthrie and Fink, 1991). The PCR-based procedure was used to construct yeast strains carrying a

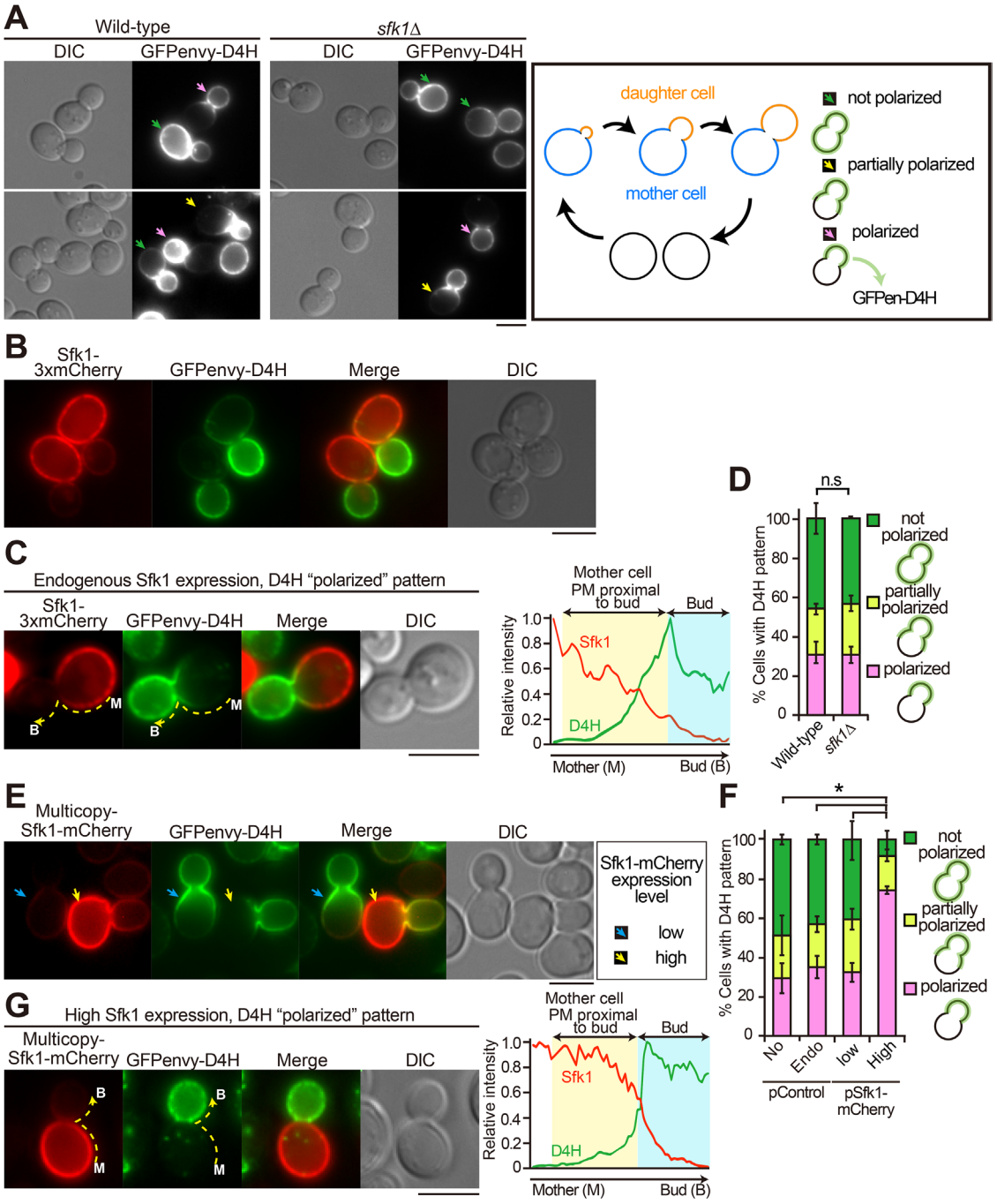

FIGURE 9: Overexpression of Sfk1 excludes GFPenvy-D4H from the mother cell PM. (A) The polarized distribution of GFPenvy-D4H. Wild-type or *sfk1*Δ cells carrying pRS316-GFPenvy-D4H were grown in SD-Ura medium to mid–log phase at 30°C. "Polarized," "partially polarized," and "not polarized" localizations of GFPenvy-D4H are indicated with pink, yellow, and green arrows, respectively. Right panel illustrates the budding yeast cell cycle. Three patterns of the GFPenvy-D4H localization are shown. (B) Complementary localization of GFPenvy-D4H and Sfk1-3xmCherry to daughter (bud) and mother cells, respectively. Wild-type cells expressing these proteins were grown at 30°C. To show endogenously expressed Sfk1-3xmCherry clearly, the brightness was adjusted to make it brighter. (C) Fluorescence intensity profile of a cell showing the "polarized" pattern of GFPenvy-D4H. Fluorescence signals were quantified along the dotted line from the mother cell to the bud. The brightness of Sfk1-3xmCherry was adjusted as in B. (D) Quantification of three GFPenvy-D4H localization patterns. The cells in A were examined. The percentage of cells showing "polarized," "partially polarized," and "not polarized" localizations of GFPenvy-D4H was determined as described in *Materials and Methods* and is expressed as the mean ± SD of three independent experiments ($n > 150$ cells in total for each strain). "n.s." indicates no significant difference between all combinations as determined by a two-tailed Student's *t* test. (E) Heterogeneous (high and low) expression of Sfk1-mCherry by a multicopy plasmid. Wild-type cells carrying pRS316-GFPenvy-D4H and YEplac181-*SFK1-mCherry* were grown in SD-Leu-Ura medium to mid–log phase at 30°C. The brightness was not adjusted after background subtraction. Arrows indicate cells highly (yellow) and lowly (cyan) expressing Sfk1-mCherry. (F) High expression of Sfk1-mCherry significantly increased the "polarized" pattern of

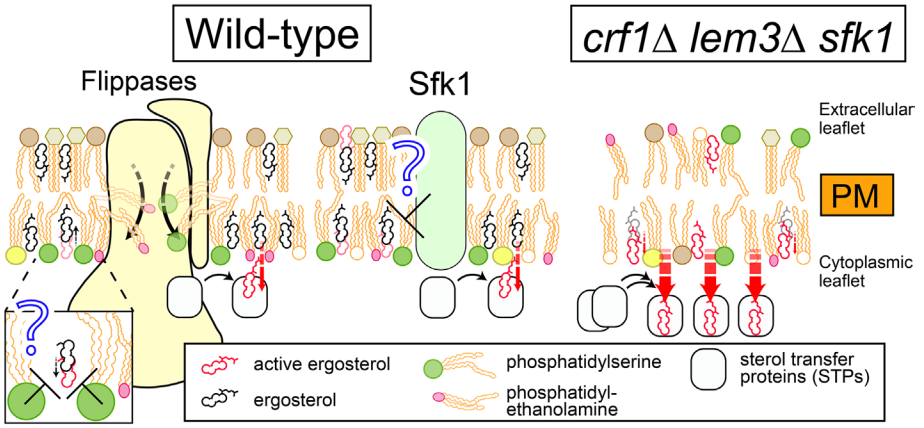

FIGURE 10: Model for the coordinated actions of flippases and Sfk1 in the control of PM sterol. PS and PE are retained in the cytoplasmic leaflet of the PM by flippases. PS has a high affinity for ergosterol because of its large head, which may shield sterol molecules from sterol transfer proteins (STPs). Sfk1 might decrease active ergosterol by unknown mechanisms. Thus, flippases and Sfk1 coordinately hold sterols within the membrane interior to limit the accessibility of sterols to the cytoplasm. In the *crf1Δ lem3Δ sfk1* triple mutant, the simultaneous loss of these proteins results in reduced shielding by phospholipids, leading to a vast increase of active ergosterol, which is likely highly accessible to and easily extracted by STPs, resulting in the loss of ergosterol from the PM.

complete gene deletion or a gene fusion with either GFP or mCherry (Longtine *et al.*, 1998; Shaner *et al.*, 2004). The amplified DNA fragments were introduced into the appropriate strains, and transformants were selected on appropriate plate media. Yeast transformations were performed using the lithium acetate method (Gietz and Woods, 2002; Gietz and Schiestl, 2007). All constructs that were produced by the PCR-based procedure were verified by colony PCR to confirm that the replacement or insertion occurred at the expected locus.

When the cell growth phenotype was examined by spot assay, cells were cultured in the appropriate medium overnight and adjusted to OD_{600} = 0.64, and then 10-fold serial dilutions were spotted onto the indicated plates. The dose-response growth curve experiment for sensitivity to duramycin was performed essentially as described previously (Takar *et al.*, 2016). The sigmoidal curve fitting was analyzed by using an analysis tool in ImageJ.

Strains carrying *3xGFP* or *3xmCherry* at genomic loci were constructed as follows. pBluescript SK+ (pBSK)-*3xGFP-Candida albicans URA3* (*CaURA3*) was constructed by subcloning *3xGFP* from pBSK-*SJL2-3xGFP* (Lee *et al.*, 2003; Sun *et al.*, 2007) (a gift from D. G. Drubin), *ADH1* terminator, and *CaURA3* into pBSK. Then, a DNA fragment of *VPH1* or *DNF3*, which encodes the C-terminal region, was inserted upstream of *3xGFP* in pBSK-*3xGFP-CaURA3*. The resulting plasmids were linearized by cutting at a unique restriction enzyme site in the target gene, followed by transformation into yeast strains. Stable URA^+ transformants were selected and screened for proper targeting by colony PCR. pBSK-*SFK1-3xmCherry-CaURA3* was constructed by replacing *DNF3* and *3xGFP* with *SFK1* and *3xmCherry*, respectively. After stable *SFK1-3xmCherry::CaURA3* transformants were obtained, *CaURA3* was replaced with the *KanMX6* cassette by marker fragment transformation. The functionality of *DNF3-3xGFP/CRF1-GFP* and *SFK1-3xmCherry* was confirmed by normal growth in the *lem3Δ sfk1Δ* and *lem3Δ crf1Δ* mutants containing these genes, respectively.

GFP-evt-2PH and *upc2-1* were cloned into pRS306-based vectors and expressed at the *URA3* locus as follows. pRS306-P_{TPI1}-GFP-evt-2PH-T_{ADH1} was constructed by replacing mCherry of pRS306-P_{TPI1}-mCherry-evt-2PH-T_{ADH1} (Miyasaka *et al.*, 2020) with GFP. The *upc2-1* (G888D) mutant fragment (–800 to +380 base pairs of the *UPC2* gene) was generated by the standard two-step PCR mutagenesis technique and inserted into pRS306. These plasmids were linearized by cutting at a unique restriction enzyme site in *URA3* and inserted into the *URA3* locus.

To express *OSH* genes on a multicopy plasmid, DNA sequences encoding *OSH* genes were amplified by PCR and subcloned into either YEplac195, YEplac195-*KanMX6*, or YEplac181 plasmids. Sterol binding–deficient *KES1* mutants (Im *et al.*, 2005) were generated by the standard two-step PCR mutagenesis technique and subcloned into YEplac195. To express the *SFK1-mCherry* fusion gene on a multicopy plasmid, the *SFK1-mCherry* fragment was generated by overlap extension PCR and subcloned into YEplac181.

To express GFP-D4H and GFPenvy-D4H in *Escherichia coli*, the D4H ($D4^{D434S}$) mutant fragment was generated by the standard two-step PCR mutagenesis technique using pColdI-mCherry-D4 as a template (Kishimoto *et al.*, 2020). The GFP and D4H fragments were inserted into pColdI (Takara Bio, Shiga, Japan) to construct pColdI-GFP-D4H. To construct pColdI-GFPenvy-D4H, GFPenvy DNA (Slubowski *et al.*, 2015) was newly synthesized with codon optimization for *Saccharomyces cerevisiae* (GeneArt Strings; Thermo Scientific, Carlsbad, CA) and amplified by PCR. pColdI-GFPenvy-D4H was constructed by replacing GFP in pColdI-GFP-D4H with this GFPenvy fragment. To express GFP-D4H and GFPenvy-D4H in yeast, the corresponding DNA fragments were inserted into pRS316-P_{TPI1}-T_{ADH1}.

Schemes detailing the construction of plasmids are available on request.

Isolation of ts mutations of *SFK1*

The ts *sfk1-2* strain was constructed by PCR-based random mutagenesis as follows. The approximately 1.2 kbp *SFK1* DNA fragment,

GFPenvy-D4H. Cells were examined and categorized as in D. Low or high expression of Sfk1-mCherry was determined as described in the legend of Supplemental Figure 10B. Bars: No, control plasmid; Endo, endogenous expression of Sfk1-3xmCherry; Low, multicopy plasmid of *SFK1-mCherry* but low expression of Sfk1-mCherry; High, multicopy plasmid of *SFK1-mCherry* and high expression of Sfk1-mCherry. The percentage of cells showing the indicated patterns is expressed as the mean ± SD of three independent experiments (n > 103 cells in total for each strain). An asterisk indicates a significant difference, as determined by the Tukey–Kramer test (p < 0.05), in the "polarized" and "not polarized" patterns. (G) GFPenvy-D4H was exclusively distributed to the bud in a cell highly expressing Sfk1-mCherry. The brightness is not adjusted after background subtraction. The right panel represents the fluorescence intensity profile quantified as in C. Bars, 3 μm.

which corresponds to the region between the 40-base-pair upstream and 197-base-pair downstream sequences of the *SFK1* gene, was PCR-amplified under a mutagenic condition (Toi *et al.*, 2003) using the genomic DNA of the wild type (YKT38) as a template. On the other hand, the *Kluyveromyces lactis LEU2* (*KlLEU2*) cassette DNA fragment was PCR-amplified under standard conditions using pUG73 (Euroscarf) as a template. In these PCRs, the primers contained additional sequences, so the *SFK1* and *KlLEU2* fragments had overlapping sequences at their 3′ and 5′ regions, respectively. Then, these fragments were used for overlap extension PCR with 5′ (*SFK1*) and 3′ (*KlLEU2*) primers to generate the *SFK1-KlLEU2* fragment. This fragment was introduced into YKT2386 (*MAT*a *crf1Δ::HphMX4 lem3Δ::TRP1 SFK1-GFP::KanMX6*), and the transformants were selected at 30°C for LEU^+ first and then for G418-sensitive phenotypes. Of these transformants, 265 clones were screened for those that showed growth defects at 37°C. Eight clones were isolated and back-crossed with YKT2332 (*MATα crf1Δ::HphMX4 lem3Δ::TRP1*) three times. The *crf1Δ::HphMX4 lem3Δ::TRP1 sfk1-2::KlLEU2*, which exhibited the tightest ts phenotype, was chosen for further analyses. Sequences of PCR primers used are available on request.

Isolation of mutants synthetically lethal with the *lem3Δ sfk1Δ* mutations

Mutants synthetically lethal with *lem3Δ sfk1Δ* were isolated according to the procedures described previously (Kishimoto *et al.*, 2005). From 1×10^4 mutagenized cells screened, three single recessive mutations were identified by genetic analyses, and the corresponding wild-type genes were cloned. These genes encode *CRF1*, *DNF3*, and *ANY1*/*CFS1* (van Leeuwen *et al.*, 2016; Yamamoto *et al.*, 2017). Null mutations of these genes were confirmed to be synthetically sick or lethal with *lem3Δ sfk1Δ*.

Isolation of multicopy suppressors of the *crf1Δ lem3Δ sfk1-2* mutant

The *crf1Δ lem3Δ sfk1-2* mutant (YKT2340) was transformed with a yeast genomic DNA library constructed in the multicopy plasmid YEp24 (Botstein *et al.*, 1979). Transformants were selected on SDA-Ura plates. The plates were incubated at 25°C for 2 d and then shifted to 37°C, followed by incubation for 3 d. Approximately 1×10^6 transformants were screened, and 186 clones were isolated. To exclude clones that carried *LEM3* or *SFK1*, the sensitivity of the clones to duramycin and cycloheximide was examined (Mioka *et al.*, 2018). Plasmids were recovered from yeast and reintroduced into the original mutant to confirm the suppression of growth defects. As a result, 10 different genomic regions were found to be responsible for suppression by DNA sequencing. The clones that contained a gene relevant to phospholipid asymmetry or lipid metabolism were further analyzed, and *KES1*, *CHO1*, and *CFS1* were identified as suppressors.

Microscopic observations

For observation of proteins fused to a fluorescent protein in living cells, cells were grown under the indicated conditions to mid–log phase (OD_{600} of 0.8–1.2), collected, mounted on a microslide glass, and immediately observed. Cells were observed under a Nikon ECRIPS E800 microscope (Nikon Instech, Tokyo, Japan) as described previously (Saito *et al.*, 2004).

Staining of PE exposed to the extracellular leaflet of the PM was performed using the Bio-Ro as described previously (Mioka *et al.*, 2018). Immunofluorescence staining of Pma1 was performed as described previously (Martinez-Munoz and Kane, 2008). For staining with filipin, cells were grown in YPDA to mid–log phase and fixed with 3.8% formaldehyde for 10 min at room temperature. The fixed cells were washed twice with phosphate-buffered saline (PBS) and resuspended in PBS containing 2.5 mg/ml filipin complex (Sigma-Aldrich). After incubation at room temperature for 15 min in the dark, cells were washed with PBS once and observed with a UV filter set. For TF-Chol labeling, the cells harboring the *upc2-1* mutation were precultured overnight in YPDA and diluted into YPDA containing 0.5% Tween-80, 0.5% ethanol, and 10 μg/ml TF-Chol (Avanti Polar Lipids, Alabaster, AL). The cells were incubated at 30°C for 3 h and then shifted to 37°C, followed by 6 h of incubation. Cells were collected, washed twice with fresh SD medium, resuspended in SD medium, and observed with a GFP filter set. Nile red staining of LDs was performed as described previously with minor modifications (Verstrepen *et al.*, 2004). Five OD_{600} units of cell culture were collected and resuspended in 100 μl PBS containing 50 μg/ml Nile red (Sigma-Aldrich). After brief mixing, the cell suspension was incubated for 15 min at room temperature in the dark. Cells were collected, washed five times with PBS, resuspended in PBS, and observed with a G-2A filter set.

Endocytosis was examined by internalization of FM4-64 as described previously with minor modifications (Kishimoto *et al.*, 2005). Cells were incubated in YPDA at 30°C for 3 h and then shifted to 37°C, followed by 6 h of incubation. Four OD_{600} units of the cells were labeled with 32 μM FM4-64 (Invitrogen, Madison, WI) in YPDA on ice for 30 min and then washed once with ice-cold YPDA. Internalization of FM4-64 was initiated by the addition of prewarmed YPDA, and the cells were incubated at 37°C for 30 min, followed by microscopic observation.

Image analysis

When the PM localization of lipid biosensors (GFP-evt-2PH and TF-Chol) was examined, cells that exhibited the mean fluorescence intensity in the PM larger than 120% of the mean fluorescence intensity of cytoplasmic space were classified as showing the PM localization. In the case of GFPenvy-D4H, which exhibited the polarized distribution, the PM of the polarized region was selected and examined as described above. The PM fluorescence intensity (filipin, Bio-Ro, and Sfk1-mCherry) was analyzed using programmed macros in ImageJ as follows. 1) The background was subtracted, 2) a cell was selected and its mean fluorescence intensity was quantified ($F_{\text{whole cell}}$), 3) the cell periphery (0.2 μm width, two pixels) was selected as the PM and its mean fluorescence intensity was quantified (F_{pm}), and 4) the signal ratio of the mean $F_{\text{pm}}/F_{\text{whole cell}}$ was calculated.

To analyze the intensity profile of GFPenvy-D4H, the cell periphery was traced with a two-pixel-wide freehand line tool along the PM of the bud and mother cell. Then, the fluorescence intensity was measured and plotted. The GFPenvy-D4H localization pattern was categorized into three patterns as follows. The PM of budded cells was divided into three regions, the bud PM (bud), the mother cell PM proximal to the bud neck (proximal to bud), and the mother cell PM distal to the bud neck (distal to bud), and the mean fluorescence intensity of each region was calculated as F_{bud}, $F_{\text{proximal to bud}}$, and $F_{\text{distal to bud}}$, respectively. Then, the cells were categorized as "polarized" ($F_{\text{proximal to bud}}$ is smaller than 20% of F_{bud}), "partially polarized" ($F_{\text{proximal to bud}}$ is larger than, but $F_{\text{distal to bud}}$ is smaller than, 20% of F_{bud}), or "not polarized" ($F_{\text{distal to bud}}$ is larger than 20% of F_{bud}).

Rhodamine uptake assay

The rhodamine uptake assay was performed essentially as described previously (Mioka *et al.*, 2018).

Sucrose density gradient fractionation

Sucrose density gradient fractionation was performed as described previously (Furuta *et al.*, 2007; Georgiev *et al.*, 2011) with minor modifications. Cells were grown at 30°C to mid–log phase in 200 ml YPDA medium and collected. Cells were converted to spheroplasts with zymolyase (Nacalai Tesque, Kyoto, Japan) and broken using a multibead shocker (Yasui-Kikai, Osaka, Japan) in break buffer (0.8 M sorbitol, 20 mM HEPES at pH 7.5, 1 mM EDTA, and protease inhibitor cocktail [Nacalai Tesque]). The step gradient of sucrose was prepared with the following concentrations: 0.5 ml 60%, 2.5 ml 44%, 2 ml 40%, 1.5 ml 37%, 2 ml 34%, 2 ml 32%, 0.5 ml 29%, and 0.5 ml 22% (wt/wt) sucrose in the break buffer. The pellet was resuspended in 0.5 ml of the break buffer and loaded on top of the gradient and then centrifuged at 200,000 × *g* in the P40ST rotor (Hitachi, Tokyo, Japan) for 16 h at 4°C. Fractions (0.9 ml) were manually collected from the top of the samples. Pdr5-GFP, Pma1, and Kex2 were detected in each fraction by Western blotting with anti-GFP (Nacalai Tesque), anti-Pma1 (a gift from R. Serrano), and anti-Kex2 (a gift from S. Nothwehr) antibodies, respectively.

Lipid analysis

Cells were grown at 30°C to mid–log phase in 250 ml YPDA medium and collected. Total lipids were extracted by the Bligh and Dyer method (Bligh and Dyer, 1959). Phospholipid amounts were determined by phosphorus assay (Rouser *et al.*, 1970). For the phospholipid analysis, samples containing 200 nmol phosphates were subjected to TLC plates (Merck, Darmstadt, Germany), and phospholipids were detected as described previously (Mioka *et al.*, 2018). To detect free and esterified ergosterol, lipid extracts containing 20 nmol phosphates were subjected to high-performance TLC (Merck) separation with hexane/diethyl ether/formic acid (40:10:2, vol:vol:vol). Ergosterols were stained with a mixture of ferric chloride/sulfuric acid/acetic acid by heating (Lowry, 1968), and the spots were scanned by an image analyzer. The ergosterol content was determined by TLC-densitometric analysis using ImageJ.

Liposome sedimentation assay

Recombinant GFP-D4H and GFPenvy-D4H proteins were prepared from *E. coli* as described previously (Kishimoto *et al.*, 2020). The protein concentrations were determined by bicinchoninic acid assay. Multilamellar liposomes were prepared by combining DOPC (NOF Corporation, Tokyo, Japan) with cholesterol or ergosterol from chloroform stocks. The lipid mixture was evaporated under a stream of nitrogen gas. Then, liposome buffer (0.1 M sucrose, 20 mM HEPES at pH 7.5, 100 mM KCl, and 1 mM EDTA) was added to the dry lipids, and the suspension was vortexed to produce liposomes. D4H binding to liposomes was analyzed as described previously (Ishitsuka *et al.*, 2011) with minor modifications. Recombinant GFP- or GFPenvy-D4H protein (200 nmol) was incubated with liposomes (final total lipid concentration is 100 μM) in HEPES-buffered saline (pH 7.5) for 30 min at room temperature. Then, the mixtures were centrifuged at 21,600 × *g* for 10 min at 25°C. The pellets were washed with HEPES-buffered saline twice. The pellets were subjected to SDS–PAGE followed by Coomassie Brilliant Blue staining. For the quantification of the protein, the stained gel was scanned and analyzed by ImageJ.

Statistical analysis

Statistical comparisons of means from two samples were performed using a two-tailed Student's *t* test. To compare the means of multiple groups, statistical analyses were performed using one-way analysis of variance followed by Tukey–Kramer multiple comparisons. A p value <0.05 was regarded as significant.

ACKNOWLEDGMENTS

We thank Shan Gao for her contribution to the initial stage of this work. We also thank David G. Drubin (University of California, Berkeley) and Toshihide Kobayashi (University of Strasbourg) for plasmids, Ramon Serrano (Polytechnic University of Valencia) for the anti-Pma1 antibody, and Steven F. Nothwehr (University of Missouri) for the anti-Kex2 antibody. We thank Masato Umeda (Kyoto University) for providing Bio-Ro, Akiko Yamaji-Hasegawa (RIKEN) and Francoise Hullin-Matsuda (INSERM) for technical advice on the sterol quantification, and Tomohiko Taguchi (Tohoku University) for helpful comments on evt-2PH. This work was supported by Japanese Society for the Promotion of Science (JSPS) KAKENHI Grants JP18K06104 (T. K.), JP 21K06076 (T. K.), JP18K14645 (T. M.), and JP19K06536 (K. T.) and by the Institute for Fermentation, Osaka (T. K.). This work was partly supported by the Photo-excitonix Project at Hokkaido University.

REFERENCES

Ali MR, Cheng KH, Huang J (2007). Assess the nature of cholesterol-lipid interactions through the chemical potential of cholesterol in phosphatidylcholine bilayers. Proc Natl Acad Sci USA 104, 5372–5377.

Almeida PF (2009). Thermodynamics of lipid interactions in complex bilayers. Biochim Biophys Acta 1788, 72–85.

Andersen JP, Vestergaard AL, Mikkelsen SA, Mogensen LS, Chalat M, Molday RS (2016). P4-ATPases as phospholipid flippases—structure, function, and enigmas. Front Physiol 7, 275.

Antonny B, Bigay J, Mesmin B (2018). The oxysterol-binding protein cycle: burning off PI(4)P to transport cholesterol. Annu Rev Biochem 87, 809–837.

Audhya A, Emr SD (2002). Stt4 PI 4-kinase localizes to the plasma membrane and functions in the Pkc1-mediated MAP kinase cascade. Dev Cell 2, 593–605.

Bagnat M, Chang A, Simons K (2001). Plasma membrane proton ATPase Pma1p requires raft association for surface delivery in yeast. Mol Biol Cell 12, 4129–4138.

Bajar BT, Wang ES, Lam AJ, Kim BB, Jacobs CL, Howe ES, Davidson MW, Lin MZ, Chu J (2016). Improving brightness and photostability of green and red fluorescent proteins for live cell imaging and FRET reporting. Sci Rep 6, 20889.

Barajas D, Xu K, de Castro Martin IF, Sasvari Z, Brandizzi F, Risco C, Nagy PD (2014). Co-opted oxysterol-binding ORP and VAP proteins channel sterols to RNA virus replication sites via membrane contact sites. PLoS Pathog 10, e1004388.

Beh CT, Rine J (2004). A role for yeast oxysterol-binding protein homologs in endocytosis and in the maintenance of intracellular sterol-lipid distribution. J Cell Sci 117, 2983–2996.

Bligh EG, Dyer WJ (1959). A rapid method of total lipid extraction and purification. Can J Biochem Physiol 37, 911–917.

Boeke JD, LaCroute F, Fink GR (1984). A positive selection for mutants lacking orotidine-5′-phosphate decarboxylase activity in yeast: 5-fluoro-orotic acid resistance. Mol Gen Genet 197, 345–346.

Botstein D, Falco SC, Stewart SE, Brennan M, Scherer S, Stinchcomb DT, Struhl K, Davis RW (1979). Sterile host yeasts (SHY): a eukaryotic system of biological containment for recombinant DNA experiments. Gene 8, 17–24.

Brickner JH, Fuller RS (1997). SOI1 encodes a novel, conserved protein that promotes TGN-endosomal cycling of Kex2p and other membrane proteins by modulating the function of two TGN localization signals. J Cell Biol 139, 23–36.

Bryde S, Hennrich H, Verhulst PM, Devaux PF, Lenoir G, Holthuis JC (2010). CDC50 proteins are critical components of the human class-1 P4-ATPase transport machinery. J Biol Chem 285, 40562–40572.

Caunt P, Impoolsup A, Greenfield PF (1988). Stability of recombinant plasmids in yeast. J Biotechnol 8, 173–192.

Chen CY, Ingram MF, Rosal PH, Graham TR (1999). Role for Drs2p, a P-type ATPase and potential aminophospholipid translocase, in yeast late Golgi function. J Cell Biol 147, 1223–1236.

Chung J, Nakatsu F, Baskin JM, De Camilli P (2015). Plasticity of PI4KIIIalpha interactions at the plasma membrane. EMBO Rep 16, 312–320.
Crowley JH, Leak FW Jr, Shianna KV, Tove S, Parks LW (1998). A mutation in a purported regulatory gene affects control of sterol uptake in Saccharomyces cerevisiae. J Bacteriol 180, 4177–4183.
Das A, Slaughter BD, Unruh JR, Bradford WD, Alexander R, Rubinstein B, Li R (2012). Flippase-mediated phospholipid asymmetry promotes fast Cdc42 recycling in dynamic maintenance of cell polarity. Nat Cell Biol 14, 304–310.
Daum G, Lees ND, Bard M, Dickson R (1998). Biochemistry, cell biology and molecular biology of lipids of Saccharomyces cerevisiae. Yeast 14, 1471–1510.
Decottignies A, Grant AM, Nichols JW, de Wet H, McIntosh DB, Goffeau A (1998). ATPase and multidrug transport activities of the overexpressed yeast ABC protein Yor1p. J Biol Chem 273, 12612–12622.
de Thozee CP, Cronin S, Goj A, Golin J, Ghislain M (2007). Subcellular trafficking of the yeast plasma membrane ABC transporter, Pdr5, is impaired by a mutation in the N-terminal nucleotide-binding fold. Mol Microbiol 63, 811–825.
Flanagan JJ, Tweten RK, Johnson AE, Heuck AP (2009). Cholesterol exposure at the membrane surface is necessary and sufficient to trigger perfringolysin O binding. Biochemistry 48, 3977–3987.
Frøsig MM, Costa SR, Liesche J, Østerberg JT, Hanisch S, Nintemann S, Sørensen H, Palmgren M, Pomorski TG, López-Marqués RL (2020). Pseudohyphal growth in Saccharomyces cerevisiae involves protein kinase-regulated lipid flippases. J Cell Sci 133, jcs.235994.
Furuta N, Fujimura-Kamada K, Saito K, Yamamoto T, Tanaka K (2007). Endocytic recycling in yeast is regulated by putative phospholipid translocases and the Ypt31p/32p-Rcy1p pathway. Mol Biol Cell 18, 295–312.
Gall WE, Geething NC, Hua Z, Ingram MF, Liu K, Chen SI, Graham TR (2002). Drs2p-dependent formation of exocytic clathrin-coated vesicles in vivo. Curr Biol 12, 1623–1627.
Georgiev AG, Sullivan DP, Kersting MC, Dittman JS, Beh CT, Menon AK (2011). Osh proteins regulate membrane sterol organization but are not required for sterol movement between the ER and PM. Traffic 12, 1341–1355.
Gietz RD, Schiestl RH (2007). Quick and easy yeast transformation using the LiAc/SS carrier DNA/PEG method. Nat Protoc 2, 35–37.
Gietz RD, Woods RA (2002). Transformation of yeast by lithium acetate/single-stranded carrier DNA/polyethylene glycol method. Methods Enzymol 350, 87–96.
Gnügge R, Rudolf F (2017). Saccharomyces cerevisiae shuttle vectors. Yeast 34, 205–221.
Greenspan P, Mayer EP, Fowler SD (1985). Nile red: a selective fluorescent stain for intracellular lipid droplets. J Cell Biol 100, 965–973.
Guthrie C, Fink GR (1991). Guide to Yeast Genetics and Molecular Biology, San Diego: Academic Press.
Hachiro T, Yamamoto T, Nakano K, Tanaka K (2013). Phospholipid flippases Lem3p-Dnf1p and Lem3p-Dnf2p are involved in the sorting of the tryptophan permease Tat2p in yeast. J Biol Chem 288, 3594–3608.
Hankins HM, Baldridge RD, Xu P, Graham TR (2015). Role of flippases, scramblases and transfer proteins in phosphatidylserine subcellular distribution. Traffic 16, 35–47.
Heese-Peck A, Pichler H, Zanolari B, Watanabe R, Daum G, Riezman H (2002). Multiple functions of sterols in yeast endocytosis. Mol Biol Cell 13, 2664–2680.
Holthuis JC, Menon AK (2014). Lipid landscapes and pipelines in membrane homeostasis. Nature 510, 48–57.
Hua Z, Fatheddin P, Graham TR (2002). An essential subfamily of Drs2p-related P-type ATPases is required for protein trafficking between Golgi complex and endosomal/vacuolar system. Mol Biol Cell 13, 3162–3177.
Im YJ, Raychaudhuri S, Prinz WA, Hurley JH (2005). Structural mechanism for sterol sensing and transport by OSBP-related proteins. Nature 437, 154–158.
Ishitsuka R, Saito T, Osada H, Ohno-Iwashita Y, Kobayashi T (2011). Fluorescence image screening for chemical compounds modifying cholesterol metabolism and distribution. J Lipid Res 52, 2084–2094.
Iwamoto K, Kobayashi S, Fukuda R, Umeda M, Kobayashi T, Ohta A (2004). Local exposure of phosphatidylethanolamine on the yeast plasma membrane is implicated in cell polarity. Genes Cells 9, 891–903.
Jandrositz A, Petschnigg J, Zimmermann R, Natter K, Scholze H, Hermetter A, Kohlwein SD, Leber R (2005). The lipid droplet enzyme Tgl1p hydrolyzes both steryl esters and triglycerides in the yeast, Saccharomyces cerevisiae. Biochim Biophys Acta 1735, 50–58.
Johnson BB, Moe PC, Wang D, Rossi K, Trigatti BL, Heuck AP (2012). Modifications in perfringolysin O domain 4 alter the cholesterol concentration threshold required for binding. Biochemistry 51, 3373–3382.
Kato U, Emoto K, Fredriksson C, Nakamura H, Ohta A, Kobayashi T, Murakami-Murofushi K, Kobayashi T, Umeda M (2002). A novel membrane protein, Ros3p, is required for phospholipid translocation across the plasma membrane in Saccharomyces cerevisiae. J Biol Chem 277, 37855–37862.
Kato U, Inadome H, Yamamoto M, Emoto K, Kobayashi T, Umeda M (2013). Role for phospholipid flippase complex of ATP8A1 and CDC50A proteins in cell migration. J Biol Chem 288, 4922–4934.
Kishimoto T, Ishitsuka R, Kobayashi T (2016). Detectors for evaluating the cellular landscape of sphingomyelin- and cholesterol-rich membrane domains. Biochim Biophys Acta 1861, 812–829.
Kishimoto T, Tomishige N, Murate M, Ishitsuka R, Schaller H, Mely Y, Ueda K, Kobayashi T (2020). Cholesterol asymmetry at the tip of filopodia during cell adhesion. FASEB J 34, 6185–6197.
Kishimoto T, Yamamoto T, Tanaka K (2005). Defects in structural integrity of ergosterol and the Cdc50p-Drs2p putative phospholipid translocase cause accumulation of endocytic membranes, onto which actin patches are assembled in yeast. Mol Biol Cell 16, 5592–5609.
Klug L, Daum G (2014). Yeast lipid metabolism at a glance. FEMS Yeast Res 14, 369–388.
Kobayashi T, Menon AK (2018). Transbilayer lipid asymmetry. Curr Biol 28, R386-R391.
Kurat CF, Natter K, Petschnigg J, Wolinski H, Scheuringer K, Scholz H, Zimmermann R, Leber R, Zechner R, Kohlwein SD (2006). Obese yeast: triglyceride lipolysis is functionally conserved from mammals to yeast. J Biol Chem 281, 491–500.
Lange Y, Steck TL (2008). Cholesterol homeostasis and the escape tendency (activity) of plasma membrane cholesterol. Prog Lipid Res 47, 319–332.
Lange Y, Steck TL (2016). Active membrane cholesterol as a physiological effector. Chem Phys Lipids 199, 74–93.
Lange Y, Tabei SM, Ye J, Steck TL (2013). Stability and stoichiometry of bilayer phospholipid-cholesterol complexes: relationship to cellular sterol distribution and homeostasis. Biochemistry 52, 6950–6959.
Lee S, Uchida Y, Wang J, Matsudaira T, Nakagawa T, Kishimoto T, Mukai K, Inaba T, Kobayashi T, Molday RS, *et al*. (2015). Transport through recycling endosomes requires EHD1 recruitment by a phosphatidylserine translocase. EMBO J 34, 669–688.
Lee WL, Oberle JR, Cooper JA (2003). The role of the lissencephaly protein Pac1 during nuclear migration in budding yeast. J Cell Biol 160, 355–364.
Lev S (2010). Non-vesicular lipid transport by lipid-transfer proteins and beyond. Nat Rev Mol Cell Biol 11, 739–750.
Lewis MJ, Nichols BJ, Prescianotto-Baschong C, Riezman H, Pelham HR (2000). Specific retrieval of the exocytic SNARE Snc1p from early yeast endosomes. Mol Biol Cell 11, 23–38.
Lewis TL, Keesler GA, Fenner GP, Parks LW (1988). Pleiotropic mutations in Saccharomyces cerevisiae affecting sterol uptake and metabolism. Yeast 4, 93–106.
Li Y, Prinz WA (2004). ATP-binding cassette (ABC) transporters mediate nonvesicular, raft-modulated sterol movement from the plasma membrane to the endoplasmic reticulum. J Biol Chem 279, 45226–45234.
Longtine MS, McKenzie A 3rd, Demarini DJ, Shah NG, Wach A, Brachat A, Philippsen P, Pringle JR (1998). Additional modules for versatile and economical PCR-based gene deletion and modification in Saccharomyces cerevisiae. Yeast 14, 953–961.
Lowry RR (1968). Ferric chloride spray detector for cholesterol and cholesteryl esters on thin-layer chromatograms. J Lipid Res 9, 397.
Maekawa M, Fairn GD (2015). Complementary probes reveal that phosphatidylserine is required for the proper transbilayer distribution of cholesterol. J Cell Sci 128, 1422–1433.
Malinska K, Malinsky J, Opekarova M, Tanner W (2004). Distribution of Can1p into stable domains reflects lateral protein segregation within the plasma membrane of living S. cerevisiae cells. J Cell Sci 117, 6031–6041.
Manik MK, Yang H, Tong J, Im YJ (2017). Structure of yeast OSBP-related protein Osh1 reveals key determinants for lipid transport and protein targeting at the nucleus-vacuole junction. Structure 25, 617–629.e613.
Marek M, Vincenzetti V, Martin SG (2020). Sterol biosensor reveals LAM-family Ltc1-dependent sterol flow to endosomes upon Arp2/3 inhibition. J Cell Biol 219, e202001147.
Martinez-Munoz GA, Kane P (2008). Vacuolar and plasma membrane proton pumps collaborate to achieve cytosolic pH homeostasis in yeast. J Biol Chem 283, 20309–20319.

Maxfield FR, Menon AK (2006). Intracellular sterol transport and distribution. Curr Opin Cell Biol 18, 379–385.
McConnell HM, Radhakrishnan A (2003). Condensed complexes of cholesterol and phospholipids. Biochim Biophys Acta 1610, 159–173.
Menon AK (2018). Sterol gradients in cells. Curr Opin Cell Biol 53, 37–43.
Mesmin B, Maxfield FR (2009). Intracellular sterol dynamics. Biochim Biophys Acta 1791, 636–645.
Mioka T, Fujimura-Kamada K, Mizugaki N, Kishimoto T, Sano T, Nunome H, Williams DE, Andersen RJ, Tanaka K (2018). Phospholipid flippases and Sfk1p, a novel regulator of phospholipid asymmetry, contribute to low permeability of the plasma membrane. Mol Biol Cell 29, 1203–1218.
Mioka T, Fujimura-Kamada K, Tanaka K (2014). Asymmetric distribution of phosphatidylserine is generated in the absence of phospholipid flippases in Saccharomyces cerevisiae. Microbiologyopen 3, 803–821.
Miyasaka M, Mioka T, Kishimoto T, Itoh E, Tanaka K (2020). A complex genetic interaction implicates that phospholipid asymmetry and phosphate homeostasis regulate Golgi functions. PLoS One 15, e0236520.
Munn AL, Heese-Peck A, Stevenson BJ, Pichler H, Riezman H (1999). Specific sterols required for the internalization step of endocytosis in yeast. Mol Biol Cell 10, 3943–3957.
Munn AL, Stevenson BJ, Geli MI, Riezman H (1995). end5, end6, and end7: mutations that cause actin delocalization and block the internalization step of endocytosis in Saccharomyces cerevisiae. Mol Biol Cell 6, 1721–1742.
Murate M, Abe M, Kasahara K, Iwabuchi K, Umeda M, Kobayashi T (2015). Transbilayer distribution of lipids at nano scale. J Cell Sci 128, 1627–1638.
Nagata S, Sakuragi T, Segawa K (2020). Flippase and scramblase for phosphatidylserine exposure. Curr Opin Immunol 62, 31–38.
Nakano K, Yamamoto T, Kishimoto T, Noji T, Tanaka K (2008). Protein kinases Fpk1p and Fpk2p are novel regulators of phospholipid asymmetry. Mol Biol Cell 19, 1783–1797.
Nelson LD, Johnson AE, London E (2008). How interaction of perfringolysin O with membranes is controlled by sterol structure, lipid structure, and physiological low pH: insights into the origin of perfringolysin O-lipid raft interaction. J Biol Chem 283, 4632–4642.
Neumann J, Rose-Sperling D, Hellmich UA (2017). Diverse relations between ABC transporters and lipids: an overview. Biochim Biophys Acta 1859, 605–618.
Noji T, Yamamoto T, Saito K, Fujimura-Kamada K, Kondo S, Tanaka K (2006). Mutational analysis of the Lem3p-Dnf1p putative phospholipid-translocating P-type ATPase reveals novel regulatory roles for Lem3p and a carboxyl-terminal region of Dnf1p independent of the phospholipid-translocating activity of Dnf1p in yeast. Biochem Biophys Res Commun 344, 323–331.
Nyholm TKM, Jaikishan S, Engberg O, Hautala V, Slotte JP (2019). The affinity of sterols for different phospholipid classes and its impact on lateral segregation. Biophys J 116, 296–307.
Panatala R, Hennrich H, Holthuis JC (2015). Inner workings and biological impact of phospholipid flippases. J Cell Sci 128, 2021–2032.
Parsons AB, Lopez A, Givoni IE, Williams DE, Gray CA, Porter J, Chua G, Sopko R, Brost RL, Ho CH, *et al.* (2006). Exploring the mode-of-action of bioactive compounds by chemical-genetic profiling in yeast. Cell 126, 611–625.
Paulusma CC, Groen A, Kunne C, Ho-Mok KS, Spijkerboer AL, Rudi de Waart D, Hoek FJ, Vreeling H, Hoeben KA, van Marle J, *et al.* (2006). Atp8b1 deficiency in mice reduces resistance of the canalicular membrane to hydrophobic bile salts and impairs bile salt transport. Hepatology 44, 195–204.
Peters C, Bayer MJ, Buhler S, Andersen JS, Mann M, Mayer A (2001). Trans-complex formation by proteolipid channels in the terminal phase of membrane fusion. Nature 409, 581–588.
Pomorski T, Lombardi R, Riezman H, Devaux PF, van Meer G, Holthuis JC (2003). Drs2p-related P-type ATPases Dnf1p and Dnf2p are required for phospholipid translocation across the yeast plasma membrane and serve a role in endocytosis. Mol Biol Cell 14, 1240–1254.
Pruyne D, Legesse-Miller A, Gao L, Dong Y, Bretscher A (2004). Mechanisms of polarized growth and organelle segregation in yeast. Annu Rev Cell Dev Biol 20, 559–591.
Puts CF, Panatala R, Hennrich H, Tsareva A, Williamson P, Holthuis JC (2012). Mapping functional interactions in a heterodimeric phospholipid pump. J Biol Chem 287, 30529–30540.
Quazi F, Molday RS (2011). Lipid transport by mammalian ABC proteins. Essays Biochem 50, 265–290.
Radhakrishnan A, Goldstein JL, McDonald JG, Brown MS (2008). Switch-like control of SREBP-2 transport triggered by small changes in ER cholesterol: a delicate balance. Cell Metab 8, 512–521.
Ramstedt B, Slotte JP (2006). Sphingolipids and the formation of sterol-enriched ordered membrane domains. Biochim Biophys Acta 1758, 1945–1956.
Rose M (1990). Methods in Yeast Genetics: A Laboratory Course Manual, ed. F. Winston and P. Hieter, Cold Spring Harbor, NY: Cold Spring Harbor Laboratory Press.
Rouser G, Fkeischer S, Yamamoto A (1970). Two dimensional thin layer chromatographic separation of polar lipids and determination of phospholipids by phosphorus analysis of spots. Lipids 5, 494–496.
Saito K, Fujimura-Kamada K, Furuta N, Kato U, Umeda M, Tanaka K (2004). Cdc50p, a protein required for polarized growth, associates with the Drs2p P-type ATPase implicated in phospholipid translocation in Saccharomyces cerevisiae. Mol Biol Cell 15, 3418–3432.
Saito K, Fujimura-Kamada K, Hanamatsu H, Kato U, Umeda M, Kozminski KG, Tanaka K (2007). Transbilayer phospholipid flipping regulates Cdc42p signaling during polarized cell growth via Rga GTPase-activating proteins. Dev Cell 13, 743–751.
Sartorel E, Barrey E, Lau RK, Thorner J (2015). Plasma membrane aminoglycerolipid flippase function is required for signaling competence in the yeast mating pheromone response pathway. Mol Biol Cell 26, 134–150.
Savinov SN, Heuck AP (2017). Interaction of cholesterol with perfringolysin O: what have we learned from functional analysis? Toxins (Basel) 9, 381.
Schneiter R, Brugger B, Sandhoff R, Zellnig G, Leber A, Lampl M, Athenstaedt K, Hrastnik C, Eder S, Daum G, *et al.* (1999). Electrospray ionization tandem mass spectrometry (ESI-MS/MS) analysis of the lipid molecular species composition of yeast subcellular membranes reveals acyl chain-based sorting/remodeling of distinct molecular species en route to the plasma membrane. J Cell Biol 146, 741–754.
Segawa K, Kurata S, Yanagihashi Y, Brummelkamp TR, Matsuda F, Nagata S (2014). Caspase-mediated cleavage of phospholipid flippase for apoptotic phosphatidylserine exposure. Science 344, 1164–1168.
Serrano R, Kielland-Brandt MC, Fink GR (1986). Yeast plasma membrane ATPase is essential for growth and has homology with (Na++ K+), K+- and Ca2+-ATPases. Nature 319, 689–693.
Shaner NC, Campbell RE, Steinbach PA, Giepmans BN, Palmer AE, Tsien RY (2004). Improved monomeric red, orange and yellow fluorescent proteins derived from Discosoma sp. red fluorescent protein. Nat Biotechnol 22, 1567–1572.
Shimada Y, Maruya M, Iwashita S, Ohno-Iwashita Y (2002). The C-terminal domain of perfringolysin O is an essential cholesterol-binding unit targeting to cholesterol-rich microdomains. Eur J Biochem 269, 6195–6203.
Slubowski CJ, Funk AD, Roesner JM, Paulissen SM, Huang LS (2015). Plasmids for C-terminal tagging in Saccharomyces cerevisiae that contain improved GFP proteins, Envy and Ivy. Yeast 32, 379–387.
Solanko LM, Sullivan DP, Sere YY, Szomek M, Lunding A, Solanko KA, Pizovic A, Stanchev LD, Pomorski TG, Menon AK, Wustner D (2018). Ergosterol is mainly located in the cytoplasmic leaflet of the yeast plasma membrane. Traffic 19, 198–214.
Steck TL, Lange Y (2010). Cell cholesterol homeostasis: mediation by active cholesterol. Trends Cell Biol 20, 680–687.
Stevens HC, Malone L, Nichols JW (2008). The putative aminophospholipid translocases, DNF1 and DNF2, are not required for 7-nitrobenz-2-oxa-1,3-diazol-4-yl-phosphatidylserine flip across the plasma membrane of Saccharomyces cerevisiae. J Biol Chem 283, 35060–35069.
Sun Y, Carroll S, Kaksonen M, Toshima JY, Drubin DG (2007). PtdIns(4,5)P2 turnover is required for multiple stages during clathrin- and actin-dependent endocytic internalization. J Cell Biol 177, 355–367.
Takahashi Y, Fujimura-Kamada K, Kondo S, Tanaka K (2011). Isolation and characterization of novel mutations in CDC50, the non-catalytic subunit of the Drs2p phospholipid flippase. J Biochem 149, 423–432.
Takar M, Wu Y, Graham TR (2016). The essential Neo1 protein from budding yeast plays a role in establishing aminophospholipid asymmetry of the plasma membrane. J Biol Chem 291, 15727–15739.
Tanaka K, Fujimura-Kamada K, Yamamoto T (2011). Functions of phospholipid flippases. J Biochem 149, 131–143.
Tanaka Y, Ono N, Shima T, Tanaka G, Katoh Y, Nakayama K, Takatsu H, Shin HW (2016). The phospholipid flippase ATP9A is required for the recycling pathway from the endosomes to the plasma membrane. Mol Biol Cell 27, 3883–3893.
Toi H, Fujimura-Kamada K, Irie K, Takai Y, Todo S, Tanaka K (2003). She4p/Dim1p interacts with the motor domain of unconventional myosins in the budding yeast, Saccharomyces cerevisiae. Mol Biol Cell 14, 2237–2249.
Uchida Y, Hasegawa J, Chinnapen D, Inoue T, Okazaki S, Kato R, Wakatsuki S, Misaki R, Koike M, Uchiyama Y, *et al.* (2011). Intracellular phosphatidylserine is essential for retrograde membrane traffic through endosomes. Proc Natl Acad Sci USA 108, 15846–15851.

van Leeuwen J, Pons C, Mellor JC, Yamaguchi TN, Friesen H, Koschwanez J, Usaj MM, Pechlaner M, Takar M, Usaj M, *et al*. (2016). Exploring genetic suppression interactions on a global scale. Science 354, aag0839.

van Meer G (2011). Dynamic transbilayer lipid asymmetry. Cold Spring Harb Perspect Biol 3, a004671.

Verstrepen KJ, Van Laere SD, Vercammen J, Derdelinckx G, Dufour JP, Pretorius IS, Winderickx J, Thevelein JM, Delvaux FR (2004). The Saccharomyces cerevisiae alcohol acetyl transferase Atf1p is localized in lipid particles. Yeast 21, 367–377.

Vida TA, Emr SD (1995). A new vital stain for visualizing vacuolar membrane dynamics and endocytosis in yeast. J Cell Biol 128, 779–792.

Yamamoto T, Fujimura-Kamada K, Shioji E, Suzuki R, Tanaka K (2017). Cfs1p, a novel membrane protein in the PQ-Loop family, isinvolved in phospholipid flippase functions in yeast. G3 (Bethesda) 7, 179–192.

Yamauchi S, Obara K, Uchibori K, Kamimura A, Azumi K, Kihara A (2015). Opt2 mediates the exposure of phospholipids during cellular adaptation to altered lipid asymmetry. J Cell Sci 128, 61–69.

Yang H, Bard M, Bruner DA, Gleeson A, Deckelbaum RJ, Aljinovic G, Pohl TM, Rothstein R, Sturley SL (1996). Sterol esterification in yeast: a two-gene process. Science 272, 1353–1356.

Yeung T, Gilbert GE, Shi J, Silvius J, Kapus A, Grinstein S (2008). Membrane phosphatidylserine regulates surface charge and protein localization. Science 319, 210–213.

Yu C, Kennedy NJ, Chang CC, Rothblatt JA (1996). Molecular cloning and characterization of two isoforms of Saccharomyces cerevisiae acyl-CoA:sterol acyltransferase. J Biol Chem 271, 24157–24163.

Zachowski A (1993). Phospholipids in animal eukaryotic membranes: transverse asymmetry and movement. Biochem J 294 (Pt 1), 1–14.